INSTITUTE OF PHYSICS PUBLISHING REPORTS ON PROGRESS IN PHYSICS

Rep. Prog. Phys. **69** (2006) 2443–2474 doi:10.1088/0034-4885/69/8/R04

Nanoscale ferroelectrics: processing, characterization and future trends

A Gruverman[1] **and A Kholkin**[2]

[1] Department of Materials Science and Engineering, North Carolina State University, Raleigh, NC 27695-7920, USA
[2] Department of Ceramics & Glass Engineering, CICECO, University of Aveiro, 3810-193 Aveiro, Portugal

E-mail: Alexei_Gruverman@ncsu.edu and kholkin@cv.ua.pt

Received 25 April 2006, in final form 12 June 2006
Published 25 July 2005
Online at stacks.iop.org/RoPP/69/2443

Abstract

This review paper summarizes recent advances in the quickly developing field of nanoscale ferroelectrics, analyses its current status and considers potential future developments. The paper presents a brief survey of the fabrication methods of ferroelectric nanostructures and investigation of the size effects by means of scanning probe microscopy. One of the focuses of the review will be the study of kinetics of nanoscale ferroelectric switching in inhomogeneous electrical and elastic fields. Another emphasis will be made on tailoring the electrical and mechanical properties of ferroelectrics with a viewpoint of fabrication of nanoscale domain structures.

This article was invited by Professor S Washburn.

Contents

1. Introduction

Ferroelectric materials exhibit a wide spectrum of functional properties, including switchable polarization, piezoelectricity, high non-linear optical activity, pyroelectricity, and non-linear dielectric behaviour. These properties are indispensable for application in electronic devices such as sensors, microactuators, infrared detectors, microwave phase filters and, ultimately, non-volatile memories [1–4]. Due to this unique combination of properties researchers and engineers have been focusing on ferroelectric materials for a long time. A number of classical monographs served as a comprehensive introduction into the field for several generations of scientists. However, recent advances in the synthesis and fabrication of micro- and nanoscale ferroelectric structures brought to life new physical phenomena that need to be studied and understood at this size range. As structure dimensions are getting smaller, ferroelectric materials exhibit a pronounced size effect manifesting itself in a significant deviation of the properties of low-dimensional structures from the bulk properties. In this sense, ferroelectrics are similar to magnetic materials since surface energy cannot be neglected in small volumes and long-range dipole interaction is significantly modified in confined geometries. However, the intrinsic size effect in ferroelectrics is considerably weaker than in ferromagnetics. This can be simply understood from a comparison of domain walls in ferroelectrics (generally several unit cells wide [5]) with much thicker Bloch domain walls in ferromagnetics. This difference is due to the fact that exchange interactions between spins are much stronger than the dipole–dipole interactions in ferroelectrics. It also depends on whether a ferroelectric is confined in one-, two-, or all three-dimensional structures. As early as 1944, Onsager [6] was able to show that in the two-dimensional lattice described by the Ising model a monolayer of non-oriented dipoles became oriented as a result of the 1st order phase transition. Many years later, rigorous experimental studies [7] confirmed the conclusion that ferroelectricity might still exist in ferroelectric films with the thickness equal to just several unit cells.

To understand the scaling behaviour, several fundamental issues need to be addressed, including the intrinsic limit for a stable domain, extrinsic effects on polarization stability, mechanism of domain wall motion and switching in nanoscale volumes. This review paper summarizes recent advances in the quickly developing field of nanoscale studies of ferroelectrics, analyses its current status and considers potential future developments. The paper begins with a brief overview of the fabrication methods of ferroelectric nanostructures, such as ultrathin films, nanocrystals, nanotubes and nanowires and investigation of the size effects and stability of the ferroelectric phase in low-dimensional structures. Application of novel characterization techniques, notably scanning probe microscopy (SPM), played a critical role in the recent advances in science and technology of nanoscale ferroelectrics [8, 9]. The paper summarizes the SPM-based methods applied for high-resolution characterization of ferroelectrics. One of the focuses of the review is the kinetics of nanoscale ferroelectric switching in inhomogeneous electrical and elastic fields probed by piezoresponse force microscopy (PFM). Recent insights into the mechanisms of ferroelectric fatigue and imprint made possible by the use of PFM are described as well. Another emphasis is made on tailoring the electrical and mechanical properties of ferroelectrics with a viewpoint of fabrication of nanoscale domain structures that can be used both for fundamental studies and for application-related purposes [10–12].

2. Ferroelectric nanostructures and size effects

Recent advances in science and technology of ferroelectrics have resulted in the development of ferroelectric structures and devices with the length scales of several hundred nanometres

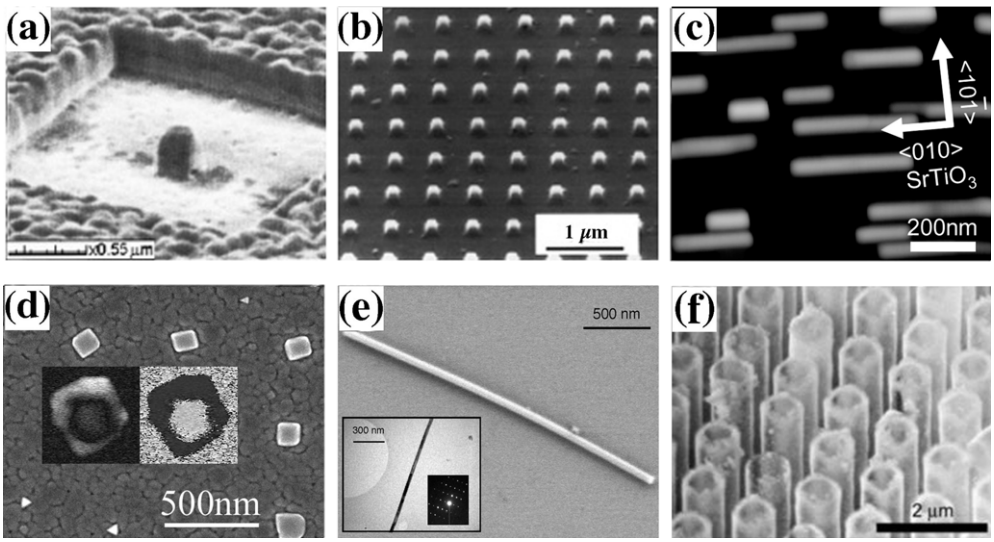

Figure 1. (*a*) Scanning ion beam image of the nanoscale PZT capacitor fabricated by FIB milling [14]; (*b*) SEM image showing a PZT cell array written by EBDW [22]; (*c*) AFM topographic image of self-assembled $PbTiO_3$ nanoislands on the Pt/$SrTiO_3$(101) substrate [30]; (*d*) PZT(100) crystallites grown on 150 wide TiO_2 seeds [35]; (*e*) SEM image of an isolated $BaTiO_3$ nanowire [16]; (*f*) a micrograph of a free-standing array of SBT tubes with diameter of about 800 nm (Image courtesy of F Morrison, University of Cambridge).

and less. Typical device examples include, but are not limited to, thin films for non-volatile ferroelectric random access memories (FeRAM), microactuators, microwave phase shifters and infrared sensors. Ferroelectrics are also considered as candidate gate-dielectric materials for field effect transistor applications due to their high permittivity. Scaling of the device dimensions to the range where ferroelectric materials start to show a pronounced size effect has emphasized the importance of nanoscale studies of ferroelectric properties. The size effect in ferroelectrics manifests itself with the reduction in the sample geometrical dimensions by a decrease in the remanent polarization, dielectric permittivity and phase transition temperature, increase in the coercive field, changes in the domain structure, etc. Until recently, high-resolution studies of ferroelectrics were limited to electron microscopy methods. Scanning probe microscopy (SPM) techniques have emerged as a powerful tool for high-resolution characterization of ferroelectrics for the first time providing an opportunity for non-destructive visualization of ferroelectric domain structures at the nanoscale. Equally important for understanding the scaling behaviour of ferroelectrics was the significant progress in the development of material processing techniques that allowed fabrication of nanoscale ferroelectric structures, such as ultrathin epitaxial films [13], nanoscale capacitors [14], nanotubes [15] and nanorods [16] (figure 1). These nanostructures can be used for studying the intrinsic size effects in ferroelectrics as well as for addressing such technologically important issues as processing damage, interfacial strain, grain size, aspect ratio effect, edge effect, domain pinning and imprint.

2.1. Ferroelectric nanocells

The ultimate goal of all the processing approaches is to develop a high-throughput, cost-effective method that would allow fabrication of large-scale regular structures with registration

precision and resolution comparable to or exceeding that of the photolithographic processes. On the way, a number of top-down and bottom-up approaches have been tried and tested, including electron-beam (EB) assisted fabrication, nanoprinting and self-assembling. The top-down methods that are widely used in modern nanotechnology provide high-precision positioning and size control but are limited in resolution. They are also prone to processing damage and are time-consuming. The bottom-up approaches allow fabrication of the structures with much smaller feature sizes but suffer from poor registration and thus require special substrate patterning that in turn involves top-down processing. A brief summary of the processing methods used for fabrication of ferroelectric nanocells is presented below.

2.1.1. Top-down approaches. EB-assisted fabrication involves patterning the ferroelectric structures either by milling of the ferroelectric layer using a focused ion beam (FIB) or by maskless EB lithography. In the FIB patterning, introduced by Stanishevsky *et al* [17], nanoscale ferroelectric capacitors have been produced by 'cutting out' an isolated island from a Pt-coated Nb-doped $Pb(Zr,Ti)O_3$ (PZT) [18] and $SrBi_2Ta_2O_9$ (SBT) [14] thin films using a 50 kV focused beam of Ga ions. Milled grooves formed a single capacitor with an isolated top metal patch (figure 1(*a*)). By optimizing the process it was possible to fabricate capacitors with lateral dimensions as small as $70 \times 70\,nm^2$. The ferroelectric properties of as-processed capacitors which showed very weak hysteresis behaviour right after processing apparently due to the Ga damage could be recovered by annealing at 600 °C. Still, the presence of a permanently damaged 10 nm thick layer has been reported.

EB-assisted fabrication, although being slow, has been instrumental in producing nanoscale ferroelectric structures suitable for studying the intrinsic size effects in ferroelectrics. One of the biggest challenges is to distinguish between these effects and damage effects caused by the fabrication process. The modified FIB milling approach developed by Nagarajan *et al* [19] allows this problem to be avoided. The FIB-milled circular holes ranging from 100 to 500 nm in diameter were created on TiO_2-coated $Pt/TiO_2/Si$ wafers followed by spin-coating deposition of sol–gel precursors that had facilitated the low-temperature (400 °C) crystallization of the $PbZr_{0.4}Ti_{0.6}O_3$ ferroelectric film. It was found that the holes served as the sites for preferential formation of the PZT crystallites with a perovskite phase. Piezoresponse force microscopy showed that the cells as small as 70–80 nm in diameter exhibited ferroelectric behaviour. The limitation of the method is that it can be used only if the ferroelectric can be crystallized below the crystallization temperature of the amorphous spun-on dielectric layer that serves as a template.

The FIB-fabricated capacitors were among the first objects where the problem of the intrinsic size effect had been addressed. Nagarajan *et al* [20] reported that the FIB-fabricated capacitors milled down to the bottom electrode exhibited a higher piezoelectric response compared with the nanocapacitors where only the top electrode was milled. This result was attributed to the reduction in the in-plane constraint in the isolated cells compared with the continuous film and thus could not be considered as the intrinsic size effect. An increase in the piezoelectric constants of the nanosize PZT single crystals was also reported by Bühlmann *et al* [21]. In this work, EB lithography with polymethylmethacrylate (PMMA) resist on the surface of the epitaxial PZT film was used to fabricate a Cr hard mask by means of a lift-off process. Ferroelectric islands with the lateral size in the range from 1 μm down to 100 nm were next produced by reactive ion etching (RIE). The piezoelectric response of the islands showed a steep (up to 300%) increase below the lateral size of 300 nm which was explained by a decrease in the fraction of *a*-domains upon scaling the feature size resulting in reduced mechanical constraint. The coercive field was found to be size-independent. In general, no

intrinsic variations in the ferroelectric properties were observed down to the $100 \times 100\,nm^2$ cell dimension.

One of the ways to counteract the low throughput of FIB patterning is the use of e-beam direct writing (EBDW) [22] which allows fabrication of ferroelectric nanocells of similar dimensions but on a large scale. In this approach, a metalorganic film deposited on a conductive substrate is irradiated locally with an electron beam with subsequent developing and dissolving of the unexposed areas. Annealing and crystallization transforms the produced metalorganic mesas into the ferroelectric cells of the well-defined shape and dimension. Using this method, arrays of $100 \times 100\,nm^2$ cells of $Pb(Zr,Ti)O_3$ (PZT) and $SrBi_2Ta_2O_9$ (SBT) have been successfully fabricated (figure 1(*b*)).

Development of various lithography-based techniques and nanoscale masks allowed further progress in the fabrication of large-scale two-dimensional periodic arrays of ferroelectric cells with well-defined dimensions. One of the most promising is imprint lithography based on compression moulding to create a thickness contrast pattern in a thin resist layer on a solid substrate followed by etching. It is a low-cost, high-throughput technology that allows fabrication of nanostructures with the minimum features size in the range from ∼20 to ∼100 nm. Harnagea *et al* [23] utilized this approach to fabricate arrays of ferroelectric PZT cells by imprinting precursor gel layers deposited by chemical solution deposition on Nb-doped $SrTiO_3$ substrates. The gel films were imprinted at room temperature by applying a pressure of 1 kbar using silicon moulds. The cells were subsequently processed using the sol–gel and metalorganic decomposition (MOD) routes. It turned out that the sol–gel processed cells retained their shape down to a size of at least 300 nm and exhibited better ferroelectric properties than the MOD processed cells which is related to different crystallization mechanisms for these routes and smaller grain size achieved during sol–gel processing.

Recently, attempts to deposit perovskite oxide materials through the nanoscale shadow masks have been undertaken. This approach offers a simplified parallel patterning of the nanostructures with a reduced number of processing steps compared with the conventional photolithography. The ferroelectric materials have been deposited by pulsed laser deposition using the silicon nitride [24] or gold nanotube [25] membranes. One of the main problems is a difficulty in controlling the size and orientation of the structures, which require high-temperature post-deposition annealing. Cojocaru *et al* [26] found that the La-doped $Bi_4Ti_3O_{12}$ dots of about 150 nm in lateral size showed epitaxial relation with the $SrTiO_3$ substrate, while $BaTiO_3$ structures on the same substrate showed polycrystalline phase with very fine grains (∼30 nm). Ferroelectric properties in both structures have been confirmed by piezoresponse force microscopy testing. Optimization of the deposition and annealing conditions might allow improved switching parameters of these nanocells.

2.1.2. Bottom-up approaches. Bottom-up approaches represent an alternative route for fabrication of ferroelectric nanostructures. Self-assembling processes governed by physicochemical interactions on the surfaces overcome the low throughput and processing damage of the EB-assisted methods. In addition, the bottom-up methods are expected to produce structures with the dimensions much smaller than those achievable in the top-down approaches. The self-assembling processes have been used for fabrication of ferroelectric nanostuctures in two ways: (1) via the growth of arrays of nanoelectrodes on top of a ferroelectric film and (2) via formation of arrays of ferroelectric nanocrystals on a substrate. There are very few reports on self-patterning of the metal electrodes on a ferroelectric surface. One of the reasons that this approach has not been pursued more actively might be that ferroelectric nanocrystals can be addressed directly by the conducting SPM tip, which has the same size range, thus rendering the top electrode redundant. Alexe *et al* [27] observed

formation of self-organized arrays of crystalline conductive δ-Bi_2O_3 mesas on the surface of Bi-rich epitaxial $Bi_4Ti_3O_{12}$ films forming due to the high temperature of the substrate during deposition. The electrodes, which depending on the processing conditions range between 125 and 200 nm in lateral size, had a well-pronounced orientation correlated with the crystallographic axes of the underlying layers. If applied to ferroelectric memory, these nanoelectrodes would yield a density up to 1 Gbit. The main problem is that it is difficult to narrow the size distribution and generate the regular array of the nanoelectrodes over the large-scale area. Moreover, testing of the δ-Bi_2O_3/$Bi_4Ti_3O_{12}$ cells by means of piezoresponse force microscopy revealed significant cell-to-cell variations of the switching behaviour which could be attributed to the inhomogeneity of the Bi oxide nanoelectrodes or the ferroelectric film itself at the nanoscale level [28].

Microstructural instability at the initial growth stages of the ferroelectric thin films first reported by Seifert *et al* [29] for epitaxial $PbTiO_3$ films on $SrTiO_3$ substrates have been explored as a basis for fabrication of ferroelectric nanocells. It has been shown both theoretically and experimentally that when a grain-size to film-thickness ratio exceeds a critical value the film breaks up into isolated single-crystalline islands. This process is governed by a balance between interfacial, substrate and film–surface energies with the surface energy anisotropy strongly influencing the growth of the nanoislands. Nonomura *et al* [30] reported the formation of the three types of self-assembled $PbTiO_3$ nanoislands during MOCVD growth on Pt/$SrTiO_3$(111), (101) and (001) with characteristic lateral sizes of 40–100 nm and height ranging from 4 to 30 nm. Irrespective of the substrate orientation the triangular-shaped, triangular-prism-shaped and square-shaped nanoislands were formed by the low-energy {100} and {001} facets due to the epitaxial relationship between the substrate and the islands (figure 1(*c*)). A similar method was applied to form the triangular-shaped PZT islands 80–100 nm wide on a Pt(111)/SiO2/Si substrate by Fujisawa *et al* [31]. All these islands exhibited a clear ferroelectric behaviour without notable size effects.

To improve crystallinity of the PZT nanocells, Szafraniak *et al* [32] used a high-temperature annealing of ultrathin film deposited by chemical solution deposition (CSD) onto a single-crystalline (001)-oriented $SrTiO_3$: Nb substrate. High-temperature crystallization promoted the formation of epitaxial nanoislands of a regular shape with the height of less than 10 nm and lateral size of about 50 nm. The lateral size as well as the height of the nanocrystals could be tuned in a certain range by adjusting the initial thickness of the deposited films and by the post-deposition thermal treatment.

Based on the analysis of the shape and size of the PZT nanoislands in [32], Dawber *et al* [33] suggested that the mechanism of the self-assembly of ferroelectric nanoislands was similar to that governing the formation of Ge islands on Si(001) [34] used for fabrication of semiconductor quantum dots. The thermodynamic model of the crystallization process predicts that the interplay between the stabilizing effect of the Ge nanocrystal surfaces and the destabilizing influence of their repulsive interactions will lead to the formation of Ge nanocrystals of three different types (pyramids, domes and superdomes) with a volume distribution for a particular type being a function of coverage and crystallization temperature. Similar shaped structures were observed in both the Volmer–Weber and Stranski–Krastanow growth modes. The experimentally determined volume distribution of the PZT islands formed by CSD [32] could be fitted to the distribution function found for Ge/Si systems indicating the same mechanism of substrate mediated strain interactions [34]:

$$\ln[w_x(m)] = -\left(B_x m^{2/3} + A_x m^{1/3} + \frac{B_x^2}{4A_x} m\right). \tag{1}$$

Here w_x is the frequency of a crystal of species X with a particular volume m, B_x is a facet energy parameter, while A_x is an edge energy parameter. Contrary to the results for Ge on Si though, the experimental results for PZT showed that superdomes became dominant at higher temperatures. This might be related to a much easier generation of dislocations at high temperature used for PZT processing that favoured the superdomes, which contained multiple dislocations.

The most significant problems related to self-patterning of ferroelectric nanocells are poor registration due to the random distribution of the nucleation sites and wide cell size distribution. Regular patterning, which is necessary to address the nanoscale ferroelectric cells used in memory or any other devices, can be achieved by combining the self-assembling on a patterned template. In the method called lithography-modulated self-assembling [35], the PZT nanocrystallites have been formed in an *in situ* sputter process on the pre-defined sites determined by a pattern of TiO_2 islands created by e-beam lithography on the Pt(111)/$SrTiO_3$ substrate (figure 1(*d*)). Local enhancement of chemical affinity results in the entrapment of the PbO molecules by the TiO_2 seeds during sputtering. The shape of the PZT crystallites which have a narrow size distribution of 120–150 nm can be changed from triangular to square by adding the $PbTiO_3$ starting layer atop of the TiO_2 seeds.

2.2. *One-dimensional ferroelectric nanostructures*

Recently, there has been significant progress in the fabrication of one- and two-dimensional ferroelectric nanostructures, such as nanorods, nanoshell tubes and free-standing nanocrystals. These structures may spur the development of novel devices such as nanoscale transducers, actuators, sensors, detectors and tunable functional elements for electronic circuits.

2.2.1. Nanowires. Synthesis of ferroelectric nanowires several years ago presented a breakthrough in the fabrication of low-dimensional ferroelectric structures. $BaTiO_3$ as well as $SrTiO_3$ nanowires were synthesized by solution-phase decomposition of barium titanium isopropoxide in the presence of coordinating ligands at 280 °C [16, 36]. This reaction resulted in well-isolated single-crystalline $BaTiO_3$ rods with the diameter from 5 to 60 nm and several micrometres long (figure 1(*e*)). High-resolution transmission electron microscopy (HRTEM) analysis of the barium titanate nanorods revealed cubic perovskite structure with one of the principal axes oriented along the nanorod length. Observation of the ferroelectric behaviour in these nanowires is not without controversy: in spite of the cubic phase, it was suggested that local non-volatile polarization could be induced in the direction normal to the nanowire axis and manipulated by means of scanning probe microscopy [16]. To induce local polarization a small bias was applied to the conductive tip held at a distance of about 10 nm above a nanowire on a gold substrate. The written polarization was then probed using electrostatic force microscopy (EFM) by measuring the shift in the resonance frequency of the cantilever. One of the possibilities is that the applied field resulted in the depletion or accumulation of the charge underneath the tip without actual ferroelectric switching. *Ab initio* calculations would be extremely important in understanding the polarization switching in one-dimensional structures.

Zhang *et al* [37] used nanochannel alumina templates to fabricate PZT nanowires by the sol–gel method. The templates were immersed into the precursor solution for several hours and then heated in air at 700 °C for 30 min by using a thermal annealing furnace. After dissolving the template, isolated polycrystalline PZT nanowires of about 45 nm in diameter and 6 μm long were obtained. The cross-section HRTEM analysis showed the presence of multiple domains and PFM testing of the ferroelectric behaviour showed much stronger piezoresponse signal for the PZT nanowires compared with the ferroelectric thin films.

2.2.2. Nanotubes. Wetting of the porous templates became instrumental in fabricating another type of ferroelectric nanostructures: nanotubes (or more correctly, nanoshell tubes, as their diameter is typically of the order of several hundred nanometres or several micrometres while the wall thickness is just tens of nanometres). The materials that have been mostly used for fabrication of nanotubes are members of the perovskite group, which include PZT [15], strontium bismuth tantalate [38], barium titanate and lead titanate [39]. Initial approach based on dip-coating of the porous alumina or silicon template with appropriate precursor solution had been proposed independently by Hernandez *et al* [40] and Mishina *et al* [41] in 2002. The electrostatic interaction and capillary effect allowed filling of nanopores as small as 20 nm in diameter and uniform wetting down to a depth of 50 μm. The template could be removed after annealing, which was performed to crystallize the sol–gel into the ferroelectric phase in the case of lead titanate and into the cubic phase in the case of barium titanate. Using polymeric wetting of alumina and silicon templates Luo *et al* [15] obtained PZT and $BaTiO_3$ (BTO) tubes with diameters in the range from 50 nm to several micrometres.

Liquid source misted chemical deposition into porous Si substrate had been used by Morrison *et al* [38] to fabricate SBT tubes with diameter ranging from several hundred nanometres to 4 μm, wall thickness $<$100 nm and length of about 100 μm (figure 1(f)). The versatility of the porous template-based fabrication is emphasized by the fact that dimensions and ordering of the tubes can be easily controlled by the arrangement of the pores in the template. By using a porous photonic Si crystal as a template the large-scale periodic arrays of the straight free-standing ferroelectric nanotubes can be produced after partial removal of the template. It is suggested that ferroelectric nanotubes can be used as nanofluidic devices in ink-jet printing, nanosyringes as well as nanopositioners [38]. Attachment of the electrodes controlling the tube piezoelectric displacement is another very serious challenge. Application of the tubes to nanopositioning devices would require two pairs of outside electrodes to allow x–y movement of the tube. In this case the inner surface of the tubes need to be coated with the metal layer. This may involve several steps of wetting of the nanoporous templates, first with precursors for ferroelectric and then for metal coating resulting in the embedded nanotube structure. For nanofluidic devices application of a series of ring electrodes around the tube circumference to pump the picolitres of liquid along the nanotube length may be necessary.

The ferroelectric switching and piezoelectric properties of the nanotubes have been measured using PFM. So far, this behaviour has been tested in the individual tubes fallen on the conductive substrates, i.e. in the direction normal to the tube length. Clear piezoelectric hysteresis behaviour has been observed in the PZT nanotubes, and this observation indicates a possibility of polarization reversal in the tube radial direction. The reported value of the effective piezoelectric coefficient ($\sim$90 pm V^{-1} [15]) seems to be comparable to that of the PZT thin films. However, given the tube/tip geometry in the PFM measurements, it is difficult to quantify the piezoelectric parameters and relate them to the PZT properties. Also, within this fabrication approach the tubes are of polycrystalline structure, which presents a serious problem in terms of controlling the uniformity of their ferroelectric properties.

2.3. Size effects in ferroelectrics

Ferroelectricity is a cooperative phenomenon that arises due to the alignment of local dipole moments via both short-range chemical and long-range physical interactions. This alignment occurs at a certain transition temperature as a result of the competition between these temperature-dependent forces. This should inevitably involve a distinct size effect, i.e. decrease in transition temperature and spontaneous polarization along with the increase in the coercive field upon the reduction in the physical dimensions of ferroelectric structures. The correlation

length (which in the first approximation describes the width of the domain wall) is the parameter that plays the major role in the estimation of the range where the size effects are expected to be significant in ferroelectric materials.

From the very beginning of size effect studies, it has been realized that size effects can be of intrinsic (i.e. related to the changes in atomic polarization at small scales) and extrinsic nature. Extrinsic effects can be due to either simple modification of the structures caused by their patterning or processing (e.g. increased contribution of grain boundaries in polycrystalline materials) or more complicated effects which include the influence of inhomogeneous strain, incomplete polarization screening at the surface and defect microstructure. Most of the early studies of the size effects refer to the extrinsic ones; therefore, information is rather contradictory and scattered even for the same materials prepared with different processing routes.

For example, even in the model compound $PbTiO_3$, one of the few ferroelectrics with a pure displacive phase transition of the 1st order, the loss of the ferroelectric properties was reported for lateral dimensions from *ca* 100 to about 12 nm (see for example [42] and references therein). Most of the studies were performed on powders, where both the phase transition temperature and polarization could be estimated by calorimetry and XRD measurements. It was recognized that size effects in particulate ferroelectrics were mainly determined by the processing rather than by the decrease in the particle size itself. That is, fine powders are often made by chemical routes or by extensive milling with subsequent heat treatment. Post-annealing eliminates many defects such as hydroxyl groups and amorphous inclusions or mechanical damage. This inevitably affects the size effects in ferroelectric powders. The fact that residual strains may actually stabilize ferroelectricity in nanoscale particles has been established quite a long time ago [43] by showing that the tetragonally distorted layers in oxide ferroelectrics can persist above the Curie temperature. Later this effect has been confirmed by the existence of spontaneous polarization in powders with the mean size of *ca* 10 nm [44]. Current opinion is that, once the processing effects are eliminated, the critical dimensions in ferroelectric oxides (such as $PbTiO_3$ and $BaTiO_3$) lie in the range 5–15 nm [45].

Size effects in ferroelectric thin films are also influenced by extrinsic effects which include grain boundaries, local non-stoichiometry, lack of crystallinity and surface depletion/accumulation. In the case where the extrinsic effects are reduced, it has been found that the ferroelectric properties can still be observed in ferroelectric films of 4 unit cells (2 nm thick!) [46], thus suggesting a significant difference in the scaling behaviour in thin films and nanopowders. It is evident that such a big difference in critical size for different samples can be caused by extrinsic effects as will be discussed in the following.

Although the continuum theories are expected to be valid only at the scales much larger than the lattice constant, many of the size effects down to the nanoscale can be explained by thermodynamic approach using Landau–Ginzburg–Devonshire (LGD) formalism with proper boundary conditions [47]. Both surface term and the effect of depolarizing field that arises due to incomplete screening of the polarization at the surface can be described by considering the following form of the Gibbs free energy:

$$F = \int \left[\tfrac{1}{2}AP^2 + \tfrac{1}{4}BP^4 + \tfrac{1}{6}CP^6 + \tfrac{1}{2}D(\nabla P)^2 - E_{\mathrm{dep}}P\right] \mathrm{d}V + \int \left(\tfrac{1}{2}D\delta^{-1}P^2\right) \mathrm{d}S, \qquad (2)$$

where P is the polarization, $A = A_0(T - T_0)$ is the temperature-dependent coefficient determining Curie–Weiss temperature, B and C are the temperature-independent coefficients, D is the gradient term which is a measure of the delocalized coupling strength, δ is the extrapolation length describing the surface effects and E_{dep} is the depolarizing field. The last term in the first integral generally describes the effect of the depolarizing field on the polarization stability within the thermodynamic approach. To some extent, the depolarizing

field always exists in polar materials due to the existence of a finite separation between the polarization charge and the compensating free charge at the electrodes [48]. If polarization is constant up to the immediate vicinity of the electrode then the depolarizing field is negligibly small. However, if the polarization decays over a long distance, or if the compensating charge in metal electrodes is distributed over a finite length (Thomas–Fermi screening length), or if a low-dielectric-constant layer exists near the surface, then the depolarization field E_d can be quite large and polarization is unstable if E_d exceeds the coercive field E_c. In all these cases, the depolarizing field is proportional to remanent polarization via depolarizing factor β, i.e. $E_{dep} = \beta P_r/\varepsilon$ (ε is the dielectric constant).

The first comprehensive description of the influence of the depolarizing field using the thermodynamic approach was done by Batra *et al* [49]. It was shown that instability in ferroelectric films on semiconductor electrodes should already occur at thicknesses below 400 nm. These calculations were confirmed by measurements of the hysteresis loops in triglycine sulfate. It is important to note that the depolarizing field and the energy associated with it can be reduced by forming antiparallel 180° domains. This further complicates the evaluation of intrinsic size effects in real systems. Shih *et al* [50] introduced 180° domains in their thermodynamic approach and calculated equilibrium polarization P and domain width d by minimizing the total free-energy density with respect to both P and d. As a result, the phase transition temperature of small particles was found to be substantially lower than that of the bulk specimen in accordance with many experiments. The critical size for $BaTiO_3$ was calculated as $\approx$175 nm being somewhat larger than the experimental value.

The surface effects can also be incorporated into LGD formalism by using the second integral in equation (2) via a so-called extrapolation length δ [51]. The extrapolation length is a measure of surface ordering and describes the difference between the long-range forces at the surface and in the bulk of the system. As the overall ferroelectric instability is governed by a competition between long-range and short-range forces, both enhancement (positive extrapolation length) and suppression of polarization (negative extrapolation length) can, in principle, occur at the surface [52]. Other extrinsic effects, such as surface-induced elongation of covalent bonds (e.g. Ba–Ti bonds in $BaTiO_3$ [53]) or surface stress in spherical particles [54], should also be taken into account.

It was recently observed that the size effects in ferroelectric thin films were always accompanied not only by the decrease in the polarization and transition temperature but also by smearing of the dielectric anomaly. This effect that cannot be understood based on equation (2) and requires more rigorous treatment. One approach is to consider stress gradients due to significant mismatch strain near the film–substrate interface [55]. Stress gradient is equivalent to the external electric field due to the flexoelectric effect and thus can shift and smear out the paraelectric–ferroelectric phase transition. As was recently noted by Bratkovsky and Levanyuk [56], the surface could be considered as a defect of a 'field' type and an internal field might arise simply due to the difference in work functions of both metal electrodes or compositional inhomogeneity. This could also cause smearing the ferroelectric anomaly in thin films or an abrupt appearance of the domain structure [57].

It is obvious that continuous theories should fail while approaching the dimensions of few elementary cells, thus necessitating *ab initio* (first-principle) calculations. Recently, Junguera and Ghosez [58] performed such calculations for a fully strained $SrRuO_3/BaTiO_3/SrRuO_3$ heterostructure grown on a $SrTiO_3$ substrate. By taking into account the interface chemistry, strain relaxation and compensation of the depolarizing field in $SrRuO_3$, they found that the 'intrinsic' size effect for such heterostructures was below 2.4 nm, i.e. 6 unit cells. Thus, the domain formation was actually not needed to maintain a stable ferroelectric phase in such ultrathin films. Another interesting conclusion was made by Fu and Bellaiche [59] who

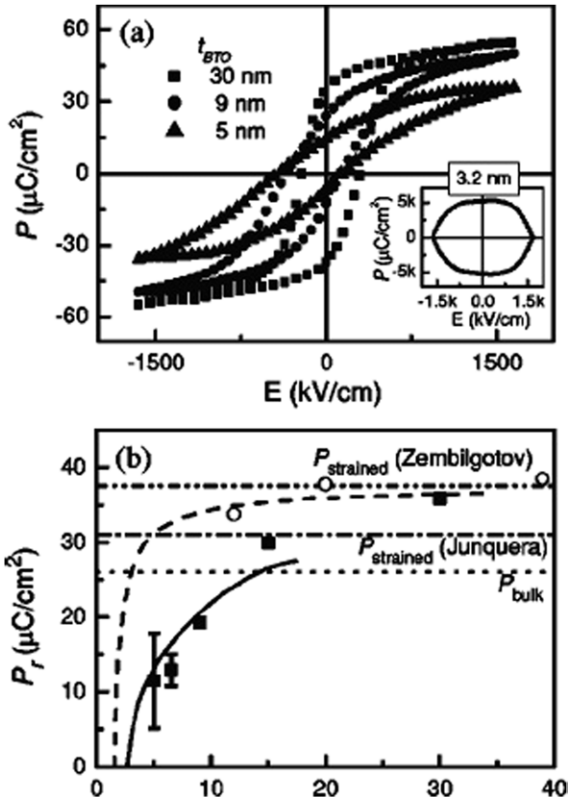

Figure 2. (*a*) P(E) hysteresis of $BaTiO_3$ films with thickness 5–30 nm and (*b*) scaling behaviour of polarization in comparison with the calculations of Junguera and Ghosez [58] and the LGD approach by Zembiglotov *et al* [61]. Reprinted with permission from [60].

predicted novel 'vortex'-type polarization state in $BaTiO_3$ quantum dots. The polarization could be still found in the dots with lateral dimensions of about 2.5 nm, where the polarization is oriented parallel to the surface, and electromechanical properties were greatly reduced. Indeed, ferroelectricity was observed in very thin $BaTiO_3$ films of about 5 nm thick [60]. Results of these measurements are shown in figure 2 along with the theoretical calculations by Junguera and Ghosez [58] and Zembiglotov *et al* [61].

It has been shown that the intrinsic size effect is insignificant even in more complex objects, such as $Pb(Zr,Ti)O_3$ thin films (∼4 nm thick) [62] and ferroelectric polymer films (∼1 nm) [63]. Due to the existence of ferroelectricity in the films of about two unit cells, the latter films are called 'two-dimensional' ferroelectrics. It has been concluded that intrinsic size effects in ferroelectric films occur at very small sizes and most of the experimental observations in 'real' ferroelectric materials are due to extrinsic effects.

3. Scanning probe microscopy techniques for nanoscale characterization of ferroelectric structures

SPM techniques have revolutionized the field of ferroelectricity, for the first time providing an opportunity for non-destructive visualization of domain structures in ferroelectric thin films and testing the nanoscale ferroelectric structures. SPM made possible nanoscale mapping

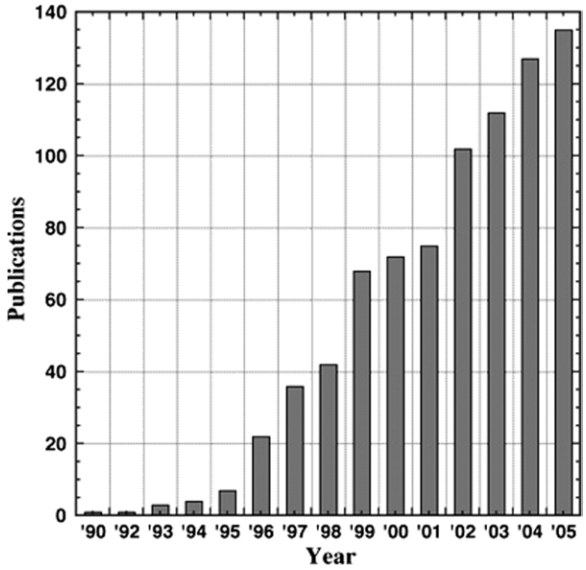

Figure 3. Number of publications on SPM studies of ferroelectrics per year. Source: ISI Science Citation Index, 2006.

of the surface potential, evaluation of local electromechanical properties, measurements of non-linear optical and dielectric constants. SPM has also opened new venues in nanoscale domain patterning for such applications as high-density data storage [12, 64] and ferroelectric lithography [10, 65]. Over the last decade a solid growth in a number of research papers on nanoscale properties of ferroelectrics studied by SPM has been observed (figure 3). Research groups in US, Europe and Asia are actively using SPM for high-resolution characterization of ferroelectric thin films, bulk ceramics, single crystals as well as for testing the scaling behaviour of ferroelectric nanostructures [66].

Depending on the type of the interaction force between the probing tip and a sample—attracting or repelling—the SPM can operate in two different regimes: non-contact or contact, respectively. In the non-contact regime, the tip is scanned over the surface at a distance of 10–100 nm, which is controlled, for example, by monitoring the resonant frequency of the cantilever [67]. The tip–sample interaction in this regime is dominated by the long-range polarization and electrostatic forces. Because of this feature, non-contact SPM can be used for ferroelectric domain imaging by detecting the electrostatic field of the surface polarization charges. This mode of SPM, called electrostatic force microscopy (EFM) [68, 69], has been predominantly applied to domain imaging in ferroelectric crystals or in thin films with micrometre-sized grains [70–79] as the lateral resolution of this technique in ambient environment is relatively low (∼40 nm). Quantitative information on local surface potential related to spontaneous polarization can be obtained by means of scanning surface potential microscopy (SSPM), or Kelvin probe force microscopy (KPFM)[80–83]. This technique provides important information on the surface electronic properties of ferroelectrics, such as distribution of polarization and screening charges and their evolution during phase transitions. Application of KPFM is essential for determining the factors that govern the stability of the ferroelectric domains and control surface electrochemical reactivity [84].

Scanning capacitance microscopy (SCM) can be used for generating an image of trapped charges by measuring local tip–sample capacitance [80, 85]. SCM is not necessarily a

non-contact mode of operation as the probing tip can be placed in direct contact with the sample surface to measure the sample capacitance. SCM can be considered as a complementary approach to KPFM in the sense that it allows the estimation of the carrier concentration in the sub-surface regions of ferroelectric samples and the evaluation of the effect of the free carriers on polarization screening. Quantitative interpretation of the SCM data is difficult since it requires an accurate account of the parameters of the dielectric layer and non-local cantilever contribution to the capacitance signal. One attractive possibility would be to use SCM and KPFM on cross-sectional samples of ferroelectric capacitors, which would allow characterization of the depletion layers in the vicinity of the film/electrode interfaces [86]. Depth profiling of the carrier concentration can be performed using a wedge-like sample by changing the lateral position of the probing tip at the slope of the wedge [87].

General drawbacks of non-contact methods include susceptibility to screening effects, sensitivity to sample surface conditions and low resolution in ambient air. The contact SPM imaging methods provide significant advantages, such as high lateral resolution (below 10 nm), a possibility of the three-dimensional reconstruction of domain structure and an effective control of nanodomains. However, interpretation of the domain images could be complicated by cross-talk between different mechanisms involved in the domain contrast formation.

Contact domain imaging methods in the contact regime can be divided into static and dynamic methods. Static imaging methods, such as atomic force microscopy (AFM) and lateral (friction) force microscopy (LFM), make use of the surface domain-dependent properties of ferroelectrics, such as surface deformations associated with the presence of different domains, difference in structure of polar faces of opposite domains, variations in friction forces, and so on [88–93]. Mechanical twinning between *a*- and *c*-domains which results in surface corrugation at the 90° domain walls allows a simple and non-destructive method for studying domain patterns in epitaxial ferroelectric films by topographic imaging of their surfaces [94, 95]. The AFM topographic mode has been also used for visualization of opposite 180° domains via detection of the static piezoelectric sample deformation induced by an external dc bias [96]. Generally, static SPM methods have limited applicability, particularly for imaging of domain structures consisting of antiparallel *c*-domains, which are of direct interest for the investigation of the polarization reversal processes in ferroelectrics.

Dynamic methods, which include scanning non-linear dielectric microscopy (SNDM) and piezoresponse force microscopy (PFM) are based on detection of the electrical and mechanical response, respectively, of the sample to an ac voltage applied via a conductive probing tip. Another dynamic contact SPM method is atomic force acoustic microscopy (AFAM) based on the detection of the cantilever displacement due to the mechanical excitation of the sample by an ultrasonic transducer which emits longitudinal waves into the sample and causes a sample surface displacement.

In the SNDM method, which employs a special resonator probe operating in the microwave frequency range [97], point-to-point detection of the local voltage-induced change in the sample capacitance allows nanoscale domain mapping in the surface layer of about 10 nm thick. It has been suggested [98] that even sub-nanometre lateral resolution can be obtained by detecting the higher order non-linear dielectric constants. However, in this case the non-linear dielectric response will be related to a much thinner surface layer. Using a slightly modified probe, it is possible to measure ε_{311} component of the dielectric tensor and thus detect the polarization component parallel to the surface potentially allowing three-dimensional reconstruction of polarization orientation [99].

The AFAM technique has been instrumental in evaluating the mechanical properties of ferroelectrics at the nanoscale, which is an important step forward for ferroelectric application

in micro- and nanoelectrical mechanical systems. In the AFAM, the cantilever vibrates at its resonant frequency while the tip remains in contact with the sample surface. Due to the size of the SPM cantilevers, the frequencies of their vibration modes are typically in the ultrasonic range. Since, the resonance frequency in contact depends on the mechanics of the tip–sample contact, variations in the elastic properties of the sample lead to a shift in the resonance frequency and to variations in the oscillation amplitude. These changes can be used either in the spectroscopic mode for quantitative evaluation of the local contact stiffness or in the scanning mode for two-dimensional mapping of the elastic properties [100]. The AFAM method has been applied to reveal the ferroelectric domains at the sub-grain level due to variations in local stiffness and to measure the elastic constants in $BaTiO_3$ [101], PZT [102–105] and $Bi_4Ti_3O_{12}$ ceramics as well as in $Pb(Mg_{1/3}Nb_{2/3})O_3$-$PbTiO_3$ single crystals [106].

Among the SPM techniques for the nanoscale characterization of ferroelectrics, by far the most popular one is piezoresponse force microscopy (PFM) [8,9,66]. Its high spatial resolution, easy implementation, effective manipulation and control of nanoscale domains and local spectroscopy capabilities make it a well-suited tool for nanoscale ferroelectric studies. The piezoresponse imaging approach makes use of the piezoelectric deformation of a ferroelectric sample in response to an external electric field (hence the term 'piezoresponse'). The linear coupling between the piezoelectric and ferroelectric constants, $d_{ij} = \varepsilon_{im} Q_{jmk} P_{sk}$, implies that the domain polarity can be determined from the sign of the field-induced strain. In the following section, we review recent advances in PFM with respect to nanoscale ferroelectric research and illustrate what information relevant to ferroelectric nanostructures can be obtained from PFM experiments.

4. Quantitative characterization of nanoscale electromechanical behaviour of ferroelectrics by PFM

Even though the PFM technique was introduced more than ten years ago, a possibility of the quantitative analysis of PFM measurements is still under debate [107–111]. The most important issues of PFM characterization include the PFM contrast formation, dynamic properties of the cantilever and contribution of the electromechanical response and electrostatic forces to the PFM signal, electroelastic field distribution inside the ferroelectric, local domain switching behaviour and PFM spectroscopy via local hysteresis loop acquisition. Some of these problems have been addressed in recently published books [8,9].

4.1. Tip–surface interaction: mechanical stress and electrostatic effect

In general, the amplitude of the cantilever vibration in the PFM mode can be presented as $A = A_{\text{piezo}} + A_{\text{cap}} + A_{nl}$, where A_{piezo} is the electromechanical response of the surface due to converse piezoelectric effect, A_{cap} is the contribution due to the electrostatic force between the tip and the sample and A_{nl} is the contribution due to non-local electrostatic force between the cantilever and the sample. Typically, when the domain size is much smaller than the cantilever length, non-local interaction results only in a constant background (offset) that can be easily subtracted from the PFM signal [110]. This allows the non-local signal to be neglected for many practical cases. One more issue is that a system composed of a conducting tip in contact with the dielectric surface on a conductive substrate can be considered as a capacitor. Therefore, an external voltage V applied between the tip and the counter electrode results in an additional capacitive (Maxwell) force that can be determined by the following equation:

$$F_{\text{cap}} = \frac{\mathrm{d}W_{\text{cap}}}{\mathrm{d}z} = \frac{1}{2} V^2 \frac{\mathrm{d}C}{\mathrm{d}z}, \tag{3}$$

where $W_{cap} = V^2C/2$ is the energy stored in the capacitor C, and z is the vertical distance. It follows that, if a combination of the dc and ac voltages, $V = V_{dc}+V_{\omega}\cos\omega t$ (V_{ω} is an amplitude of an ac voltage) is applied between the tip and the counter electrode, the capacitive force will consist of a static force F_0, a force oscillating at a driving frequency $\omega(F_w = V_{dc}V_w\,dC/dz)$, as well as a force oscillating at double frequency 2ω. These forces can be essential even in the contact mode and must be compared with other forces including contact force exerted by the cantilever and electromechanical force acting on the tip due to the piezoelectric effect. In the case where there is a contact potential difference V_c between the tip and the ferroelectric surface, the electrostatic signal can be written as $F_w = (V_{dc} - V_c)V_w\,dC/dz$ [110], i.e. the electrostatic contribution is still present even in the absence of the external bias. In addition to capacitive forces, Coulomb attractive forces between the charged surface and the tip can interfere with the local piezoelectric measurements. This effect is further complicated by the screening charges absorbed on the sample surface. In most cases it is assumed that polarization charges are completely screened and thus the electrostatic contribution can be neglected in equilibrium conditions.

Given the operation principle of the PFM method, piezoelectric materials provide an additional response to the applied ac electric field due to the converse piezoelectric effect: $\Delta z = d_{33}V$, where d_{33} is the effective longitudinal piezoelectric coefficient. It follows that both electrostatic and piezoelectric signals are linear with the applied voltage and thus contribute to the measured PFM response. These measurements are referred to as *out-of-plane* (or vertical PFM, or VPFM) measurements. As d_{33} is coupled to polarization and dielectric constant, the phase of d_{33} depends on the polarization orientation while the d_{33} magnitude is a measure of the normal component of ferroelectric polarization. Additionally, a ferroelectric grain may contract in the film plane, due to non-zero transverse piezoelectric coefficient d_{31}. If the tip is not positioned in the centre of the grain, this effect could result in a torsional movement of the cantilever even in the grain with polarization normal to the film surface. The direction of the polarization for the in-plane polarized ferroelectric grain can be deduced via a relevant (shear) piezoelectric coefficient d_{15}. In this case, the applied electric field causes a shear deformation of the grain, which is transferred via the friction forces to the cantilever torsion. These measurements are often denoted as *in-plane* (or lateral PFM, or LPFM) measurements. Generally, the vertical deflection and torsional movement of the cantilever can be used to analyse the three-dimensional polarization distribution in randomly oriented grains.

Since the signal acquired at the 1st harmonic always comprises piezoelectric and electrostatic terms, much effort was dedicated to distinguishing the conditions at which the useful piezoelectric signal related to ferroelectric polarization predominates. For example, Hong *et al* [110] compared the piezoelectric and electrostatic contributions to the signal by measuring response on both piezoelectric and non-piezoelectric surfaces at different tip–surface separations under varying dc voltage V_{dc}. They suggested that both signals could be extracted by measuring the phase of the signal that does not differ for the domains of opposite polarities. Also, the shape of the hysteresis loops could be an indicator of the electrostatic contribution. Kalinin and Bonnell [111] rigorously analysed the conditions of piezoelectric imaging in different loading force regimes by calculating the tip–surface forces due to both electromechanical and electrostatic interaction. Two limiting cases, so-called strong and weak indentation regimes, which differ in the degree of mechanical pressure exerted by the tip, were considered. It was shown that only in the strong indentation regime the total signal was directly related to d_{33}; however, the minor influence of other parameters such as dielectric constant or elastic moduli could still be notable. Piezoresponse contrast maps were constructed to correlate imaging conditions with the experimentally observed signal. It should be noted that for weak indentation forces, the electroelastic contribution to the electric field below the tip

can be neglected, since the contact area between the tip and the surface is small. In this case, the electric field in the material can be calculated using the electrostatic sphere-plane model. The high spatial resolution in this case (3–10 nm) can be achieved because the capacitance of the contact area is larger than that of the spherical part of the tip. However, the strong indentation case requires solving a coupled electroelastic problem of the spherical indentation of a piezoelectric that takes into account electrostatic, pure elastic and electroelastic interaction. This problem was recently addressed by Kalinin *et al* [112] using an elastic–piezoelectric correspondence principle.

4.2. Thermodynamics of domain switching

Applications of PFM for high-density data storage and ferroelectric lithography necessitate studies of both thermodynamics and kinetics of the switching process. The first analysis of the thermodynamics of domain switching in PFM capturing the essential features of this process including finite nucleation bias was given by Abplanalp [113]. The closed form solution for domain switching in the point charge approximation was given by Molotskii *et al* [114, 115]. Thermodynamic description of domain switching based on rigorously derived ferroelectroelastic fields was developed recently [112, 116]. Analysis of this problem was further developed by Morozovska and Eliseev [117]. In all these papers, it was shown that the spatial extent of the field produced by the tip was confined below the tip; therefore, the switching had to be limited to a small volume of material. For point charge type models with charge located on or below the ferroelectric surface, the field in the vicinity of the tip was infinite and domain nucleation was induced at arbitrarily small biases [114, 118]. In the models that considered finite tip–surface separation or that were based on realistic tip geometry [115, 116, 119], finite nucleation bias was predicted. In the former case, using exact closed form solutions for the electroelastic fields, the domain nucleation under the PFM conditions could be described in terms of the Landau theory of phase transitions [116]. In this case, the domain size played the role of the order parameter and the applied bias could be considered as a temperature.

Also, it was shown that for a point charge on the surface or inside the ferroelectric, domain nucleation could be considered as a second order phase transition. However, for the charge above the surface and for the realistic tip shape, the switching should be considered as a 1st order process. For the pure ferroelectric switching, the domain size was independent of the contact area and was determined solely by the tip charge or force. On the contrary, in the high-order ferroelectroelastic switching [120] the tip–surface contact contribution to the domain free energy dominated due to the much higher concentration of electroelastic and elastic fields below the tip. This analysis was very useful for determining the smallest possible size of the artificially created domains that could be produced for high-density data storage. Figure 4 illustrates domain sizes obtained using ferroelectric and ferroelectroelastic switching in PZT thin films and $LiNbO_3$ single crystals.

4.3. Local PFM spectroscopy

Along with the sequential polarization switching performed with a series of voltage pulses applied through the tip followed by consequent imaging, PFM has been used in a spectroscopy mode when the measurements are done in a certain location by a fixed tip (local d_{33} acquisition). This technique played a crucial role in evaluating the switching behaviour of ferroelectric nanostructures: nanocells, nanorods and nanoshell tubes. In PFM spectroscopy, a dc voltage superimposed on a high-frequency modulation voltage is swept in a cyclic manner. This

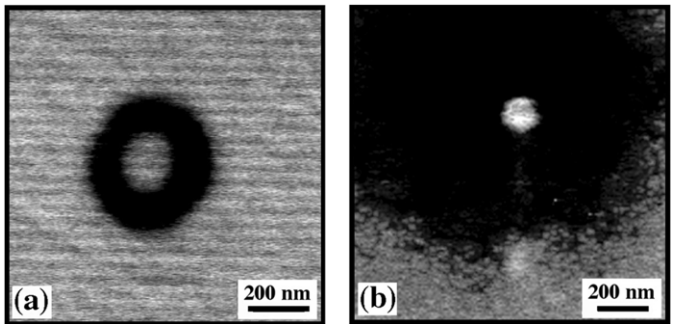

Figure 4. Artificial domains obtained by the application of a voltage bias of (*a*) −200 V to $LiNbO_3$ crystal and (*b*) −6 V to PZT thin film [116]. Small domains are due to confinement of mechanical stress exerted by the PFM tip and consequent ferroelectroelastic switching.

dependence of the local piezoelectric vibration on the applied dc bias is referred to as a piezoelectric hysteresis loop. If performed on a macroscopic scale this loop corresponds to a weak-field piezoelectric coefficient tuned by a continuously varying bias field. According to a linearized electrostriction equation, the piezoelectric coefficient can be often expressed as $d_{33} = 2Q\varepsilon_{33}P_3$, where Q is the longitudinal electrostriction coefficient and ε_{33} and P_3 are the corresponding dielectric constant and spontaneous polarization values. Therefore, the d_{33} variation reflects polarization switching with corresponding tuning of the dielectric permittivity $\varepsilon(E)$ and polarization $P(E)$, both of which affect the piezoelectric coefficient. It was observed that at the nanoscale level the shape of piezoelectric loops is different reflecting different physical mechanisms involved [121]. Measurements of local hysteresis loops are of great importance in inhomogeneous or polycrystalline ferroelectrics because they are able to quantify polarization switching on a scale significantly smaller than the grain size or inhomogeneity variation (typically several tens of nanometres).

Macroscopically, the switching occurs via the nucleation and growth of a large number of reverse domains in the situation where the applied electric field is uniform. Therefore, the d_{33} hysteresis reflects the switching averaged over the entire sample under the electrode. In the PFM experimental conditions, the electric field is strongly localized and inhomogeneous; therefore, the polarization switching starts with the nucleation of a single domain just under the tip [122]. Upon increasing the applied dc bias, this newly formed domain elongates to the bottom electrode, simultaneously expanding in lateral dimensions until reaching an equilibrium size, which depends on the value of the maximum applied voltage. The shape of the local piezoelectric hysteresis loop measured by PFM can be understood by scanning the area adjacent to the tip in between the voltage increments, provided no significant relaxation occurs [123].

An example of the visualization of the piezoelectric hysteresis in polycrystalline PZT films prepared by the sol–gel route is shown in figure 5. A sudden contrast change (arrow at V^* in figure 5) corresponds to the appearance of the stable inverse domain. Thus, nucleation voltage can be considered as an analog of the coercive voltage in local measurements rather than the voltage where $d_{33} = 0$. A rapid increase in d_{33} with increasing V_{dc} is explained by the forward and lateral growth of the nucleated domain, progressively contributing to the PFM signal. When the size of the inverse domain is much greater than the penetration depth of the weak ac field, the tip senses only a fully polarized area with aligned polarization and d_{33} is well saturated. Figure 5 also illustrates the propagation of domain wall in polycrystalline ferroelectrics where local inhomogeneity and stresses make the

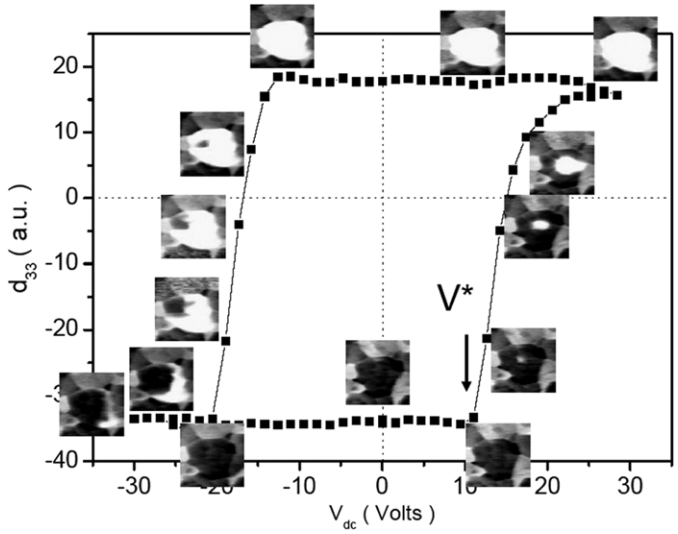

Figure 5. Local PFM hysteresis loop measured in a thick polycrystalline PZT film prepared by sol–gel. The insets (scan size 1 μm) show the static domain structures obtained by scanning with ac voltage of amplitude 1 V in the corresponding points of the hysteresis [123].

domain boundary strongly irregular. The analysis of the hysteresis loop shape was performed in the thermodynamic and kinetic approaches [124, 125]. In the thermodynamic case, the domain size is determined by the thermodynamically equilibrium state, which is a function of spontaneous polarization and domain wall energy. In the kinetic limit, the domain size is limited by the velocity of the forward and lateral domain growth. The parameters that can be extracted from the loop also include the pinning strength of the material or energy losses during switching.

5. Switching processes and ferroelectric degradation effects probed by PFM

5.1. Domain dynamics at the nanoscale

Applications of ferroelectric domain patterning for data storage, electro-optical devices and ferroelectric lithography necessitate fundamental studies of the domain switching process, kinetics of domain nucleation, growth and relaxation. Although high spatial resolution of PFM provides a unique opportunity for the investigation of domain dynamics in thin films, its poor time resolution, which is determined by the time required for image acquisition (at the scan rate of 2 Hz and image resolution of 256 $\times$ 256 pixels, it takes about 2 min to acquire an image), makes the *in situ* measurements of domain dynamics during fast switching processes difficult. While PFM can be readily used to investigate slow polarization relaxation processes with characteristic times of the order of minutes and above, it is a great challenge to deduce the mechanism of ferroelectric domain transformation when polarization reversal occurs in a matter of microseconds and faster.

This problem can be partly circumvented by studying domain dynamics in a quasi-static regime using a so-called *step-by-step switching* approach developed and applied to PFM [126]. In this approach, partial reversal of polarization is generated by applying a voltage pulse shorter than the time required for full switching but with the pulse amplitude fixed above threshold

voltage. By applying a sequence of such short pulses of incrementally increasing duration with PFM domain imaging after each pulse, a consistent picture of domain dynamics can be obtained. This approach can provide information on the domain wall velocity, its spatial anisotropy and field dependence. To describe the sidewise expansion of the domain, it is necessary to take into account the field dependence of the domain wall velocity and the spatial distribution of the electric field generated by the probing tip. An important feature of the *step-by-step switching* approach is that it can be applied both to the samples with the electrode-free surface and to the samples with deposited top electrodes (capacitors).

In the step-by-step approach, the time resolution is determined by the pulse length increment, which can be in the nanosecond range. This is particularly important from the viewpoint of studying fast switching dynamics in thin-film ferroelectric capacitors used in memory devices where the switching time is typically below 100 ns. In this case, the time resolution will also depend on the rise time of the input pulse generated by the voltage source and on the size of the capacitor, i.e. its *RC*-time constant [127].

5.1.1. Domain growth during tip-induced switching. The measurement of the size of switched domains versus the magnitude of applied voltage and time can give an insight into the mechanism of polarization switching in ferroelectric films. Although the PFM measurements are quite slow, it is possible to distinguish between different mechanisms that control the propagation of the domain wall in a complex object such as ferroelectric thin film with defects. Tybell *et al* [11] by studying the time dependence of the size of domains generated by the PFM tip in $Pb(Zr_{0.2}Ti_{0.8})O_3$ epitaxial films on $SrTiO_3$: Nb substrates could assign the motion of the domain wall to the creep mechanism. These measurements allowed calculations of the domain wall velocity as a function of the calculated electric field. Within the limitation of the point charge model, the results showed that even in a high-quality thin ferroelectric film the domain wall motion was limited by the creep mechanism with the critical exponent close to unity.

In another work, Rodriguez *et al* [128] studied the domain switching kinetics in stoichiometric $LiNbO_3$ single crystals by applying voltage pulses of different amplitudes and durations over 5 orders of magnitude. The minimum size of the created domains was much larger than in the case of thin PZT films and the mechanism of domain wall motion in this case was quite different. The domain wall velocity was calculated as a function of the domain radius by taking into account the tip-induced electric field distribution determined within the charge sphere model. It was shown that for sufficiently large domain sizes (the boundary of the growing domain is far from the tip–sample junction), the motion of the domain wall was an activation-type process, while for the small domains (domain boundary is close to the tip–sample junction) it was a non-activation process since the applied electric field was much larger than the coercive field. They suggested that the kinetics of the sidewise domain growth could be described by a universal scaling curve $g(t) = r(V, t)/V$ (where r is a radius of the growing domain and V is the tip bias). It was also suggested that this universal scaling behaviour was directly related to the field dependence of domain wall velocity and field distribution inside the material opening a way for developing a general model describing the domain switching in PFM.

5.1.2. Domain dynamics in capacitor configuration. The PFM step-by-step switching approach also allows investigation of the domain dynamics in a plane capacitor configuration where the probing tip is in contact with a thin electrode layer deposited on the sample surface. This configuration offers several advantages. First, the applied electric field is well defined, since the piezoelectrically excited region is large as compared with the tip diameter. Even for the micrometre-size thin film capacitors, the approximation of the plane capacitor

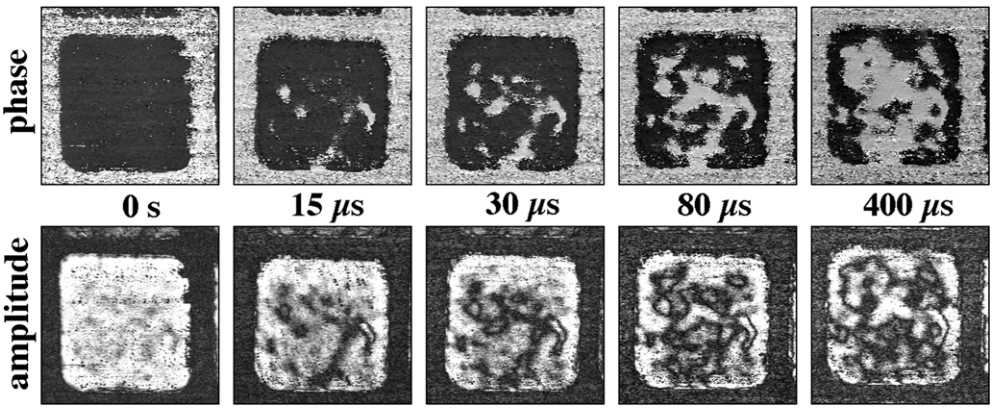

Figure 6. PFM phase and amplitude images of instantaneous domain configurations developing in the $3 \times 3\,\mu m^2$ PZT capacitor at different stages of polarization reversal under the 1.1 V bias [127].

works well and the electric field is considered homogeneous and well defined. Second, the electrical contact between the tip and the ferroelectric surface is much more reliable. Third, degradation of the tip metal coating due to the passing currents can be minimized by making an external connection to the capacitor (external connection is not possible though if capacitors of micrometre dimensions are to be measured; in this case, the tip has be used for voltage application). Fourth, the PFM results can be directly compared with the switching current data obtained by conventional measurements. The disadvantage of this technique is its inherently lower spatial resolution due to PFM domain imaging through the top electrode and possible artefacts due to the bending effect of the substrate in case of large scale electrodes (several hundred micrometres in diameter) [129].

The experimental setup developed by Dehoff *et al* [130] combines the step-by-step switching capabilities of PFM with the standard switching current measurement unit. Realization of the PFM step-by-step-switching in thin film capacitors involves partial reversal of polarization by applying a voltage pulse shorter than the capacitor's total switching time t_{sw} and with the pulse amplitude fixed above the threshold voltage. By applying a sequence of such short pulses of incrementally increasing duration ($\tau_1 < \tau_2 < \tau_3 < \cdots < t_{sw}$) with PFM domain imaging after each pulse, a consistent picture of domain dynamics can be obtained. Using this approach, direct studies of domain dynamics during polarization reversal in PZT memory capacitors were performed by Gruverman *et al* [131]. Analysis of the sequence of the domain patterns allowed elucidation of the mechanism of polarization reversal (figure 6). The forward growth velocity of domains measured directly was found to be 0.3–0.4 m s^{-1} for the voltage pulse of 1.4 V. The lateral growth velocity was also evaluated by measuring the time dependence of domain radius. Among the most revealing results were the fact that the lateral velocity was strongly inhomogeneous over the capacitor surface (it differed by 3 orders of magnitude most likely due to the interaction with microstructural defects).

Analysis of the data showed that in the fast initial stage of switching the polarization reversal proceeded via domain nucleation and, later, via the slow lateral growth. Thus, the speed limiting factors were different for the fast and slow switching stages: it was the forward growth velocity for the former and lateral growth velocity for the latter. The nucleation-dominated stage of polarization reversal could be well described by the Kolmogorov–Avrami–Ishibashi model [132–134], while at the slow switching stage a broad distribution of the relaxation times should be taken into account. It was suggested that the slow switching part could not be

detected by the standard switching current measurements (the switching current is too low), thus leading to incorrect evaluation of the switching parameters of the memory capacitors. There are a number of issues related to the development of ferroelectric memory devices that can be addressed using this approach including the effect of the top electrode perimeter and capacitor size on the switching mechanism and polarization retention.

5.1.3. Domain relaxation studies by PFM. Along with the study of the mechanisms of the domain nucleation and growth, the PFM method is also applicable to the investigation of domain relaxation [126]. The stability of the polarization state created by the external voltage is a prerequisite for the realization of SPM-based ferroelectric memories since it directly controls the retention time of the stored bits. In addition, polarization relaxation is important for the understanding of ageing phenomena in piezoelectric ceramics. The advantage of PFM as compared with macroscopic measurements of depolarization is that it allows understanding of this effect locally rather than by averaging over many backswitching events. Unfortunately, the time resolution of PFM measurements is not high enough to study the initial stages of polarization loss (within the microsecond and millisecond range).

Several studies have been recently performed on the relaxation phenomena by PFM. Despite these efforts, there is still a lack of reliable data on most ferroelectric materials useful in device applications, including the time dependence of the retention loss in ferroelectric films. While some authors reported a log linear dependence of the polarization relaxation in PZT films [135], other groups deduced a stretched exponential dependence [136] in the same material. Moreover, polarization relaxation has been found to differ in epitaxial films where a spontaneous nucleation of 180° domain walls on existing twin boundaries has been found to modify the relaxation process [137]. In this case, it was possible to use a modified Avrami–Kolmogorov–Ishibashi kinetics for the description of depolarization processes in ferroelectric thin films.

5.2. Imprint and fatigue studied by PFM

Domain studies at the nanoscale are of great practical importance for the development of high-density FeRAM devices as they allow a better understanding of mechanisms of polarization fatigue and imprint.

5.2.1. Fatigue. Fatigue is defined as a loss of switchable polarization under prolonged cycling with a strong ac or pulse voltage [1]. The problem of fatigue is quite non-trivial as it involves a complex of interrelated physical and chemical phenomena occurring mainly at the interface between the electrode and ferroelectric thin film. In the pre-SPM time, direct measurements of domain configurations developing during fatigue were impossible because of a lack of suitable techniques. Only with the advent of PFM, it became feasible to address this issue directly. In the electrode-free sample, the fatigue process is emulated by applying a high (well above the threshold value) ac voltage to the tip that scans the sample surface and thus inducing continuous switching at each point of the scanned region. After this, a dc poling is performed in the fatigued region by scanning it with the tip under a constant bias in an attempt to pole the region in one direction [138]. PFM fatigue studies both in electrode-free films [138] and in thin film capacitors [139] have showed that fatigue proceeds via region-by-region or grain-by-grain suppression of switchable polarization and is always accompanied by strong domain wall pinning, so that certain domains become frozen and do not participate in switching anymore. Figure 7 illustrates this process as a gradual decrease in the switchable area (bright contrast) due to the fatigue process. The results have been complemented by local piezoelectric hysteresis measurement that showed a progressive shift of the d_{33} loop in both vertical and horizontal

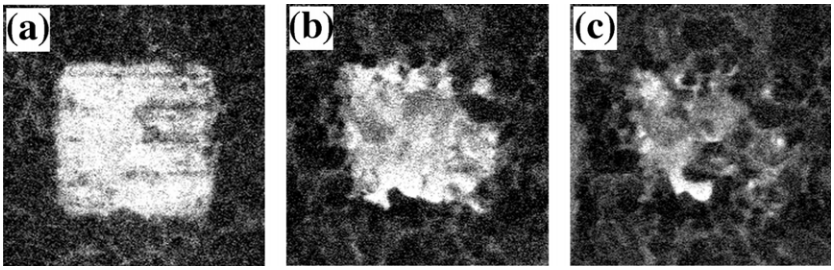

Figure 7. PFM images of the PZT/Pt heterostructure at various stages of the fatigue process. (*a*) The bright square of $1 \times 1\ \mu m^2$, produced by moving the PFM tip while applying a negative 15 V dc voltage, represents a negatively polarized region in as-grown PZT film. (*b*) and (*c*) The same film after it was fatigued by scanning for (*b*) 1 h and (*c*) 2 h with the tip held under an ac voltage of 8 V (peak-to-peak). Unswitchable crystallites appear as dark areas inside the square region that was scanned again with the tip under a negative dc 15 V bias [141].

directions (also observed by the macroscopic technique [140]). This shift corresponds to a significant imprint of the polarization state (one polarization state is preferred over the other). The orientation of the frozen domains can either have a strong preferential direction (terminated at one of the electrodes) or be randomly distributed in both directions. The size of the frozen regions varies between 100 nm to several micrometres implying critical consequences when the capacitor size is reduced to similar dimensions.

Several studies have been performed to understand the effect of fatigue after the top electrode removal [142, 143]. In this way, the lower resolution of the capacitor configuration could be circumvented. The frozen domains were also examined under different ac-voltages and it was concluded that pinned domains are localized in the vicinity of the top electrode and do not extend into the bulk of the films.

5.2.2. Imprint in ferroelectric capacitors. Another important degradation effect in ferroelectric films is the imprint defined as a preference of one polarization state over the opposite one. The most important manifestation of this effect is the shift of a hysteresis loops along the voltage axis and consequent instability of one of the polarization state even in films with symmetric electrode configuration. Nanoscale mapping of polarization distribution in the FeRAM PZT capacitors as well as local d_{33} hysteresis measurements revealed a significant difference in imprint behaviour between the peripheral and inner parts of the capacitors [144]. It was found that the inner regions of the capacitors were negatively imprinted (with the preferential direction of the normal component of polarization directed toward the top electrode) and tended to switch back after application of the positive poling voltage. On the other hand, switchable regions at the edge of the integrated capacitors generally exhibited more symmetric hysteresis behaviour. The observed effect was explained by incomplete or asymmetric switching due to the mechanical stress conditions existing in the central parts of the capacitors.

This hypothesis was tested by direct studies of the effect of mechanical stress on the capacitor switching behaviour at the nanoscale. Since domain walls in ferroelectrics are simultaneously ferroelectric and ferroelastic, the switching mechanism and domain wall kinetics is influenced by the stress state of the film arising, among other factors, due to the misfit strain between the film and the substrate. It was shown that the external stress combined with the substrate-induced strain could dramatically change the polarization state of the film [145]. PFM allowed direct observation of the domain structure behaviour under tip-induced stress [146] or

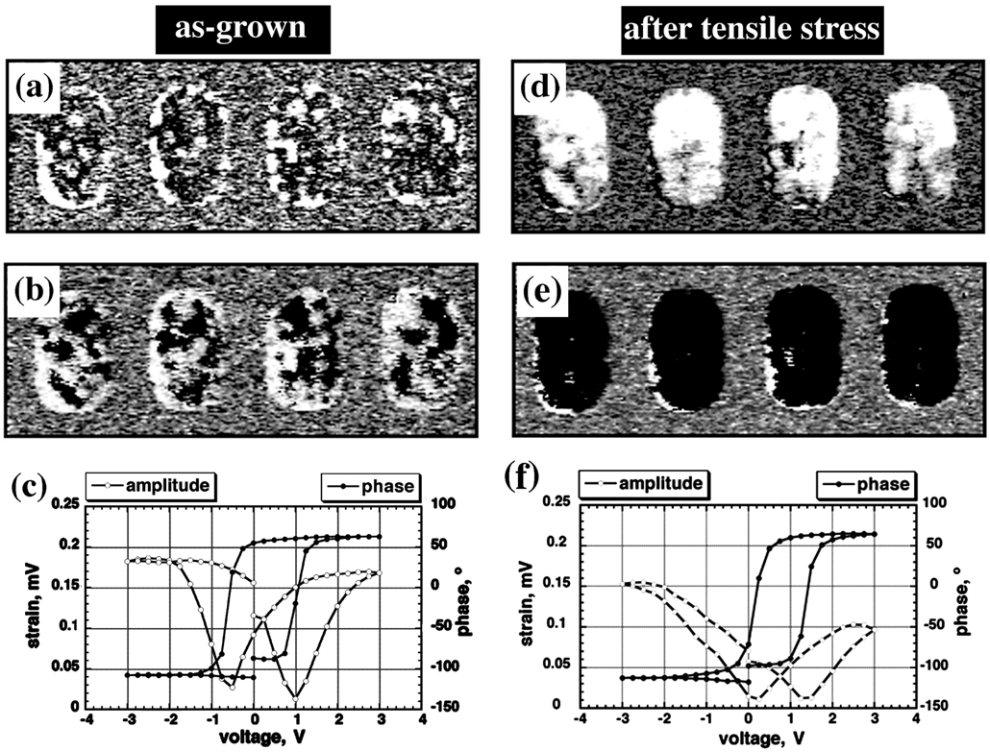

Figure 8. PFM images illustrating the influence of stress on polarization and switching behaviour of (111)-oriented PZT capacitors. (*a*) and (*d*) amplitude images, (*b*) and (*e*)—phase images, (*c*) and (*f*)—d_{33}(V) hysteresis loops [147].

macroscopic stress generated by the substrate bending [147]. In the latter study, it was found that application of external stress of the order of only 100 MPa produced complete poling of the FeRAM PZT capacitors. Figure 8 illustrates this stress-induced alteration of the domain structure in the micrometre-size PZT capacitors (black contrast on phase images after tensile stress application) along with the corresponding d_{33}(V) hysteresis loops. In addition to poling, significant imprint was induced by the mechanical stress. Stress-induced polarization direction depended on the sign of the applied stress (tensile or compressive), which was explained by the flexoelectric effect where the stress gradient, rather than the stress itself, affected the domain structure.

6. Current issues and future trends in fabrication and application of nanoscale domain patterns

The SPM capability of domain manipulation and control stimulated efforts towards generation of nanoscale domain structures that can find application in novel electronic devices and nanofabrication methods. Application of a small dc voltage between the tip and bottom electrode generates an electric field well above the threshold field of most ferroelectrics, thus inducing local polarization reversal. The problem is that in the tip–sample geometry the field is strongly inhomogeneous. Depending on the dielectric properties of the sample the characteristic length of the field decay can be in the range of several nanometres to micrometres, which apparently limits domain control to thin films and ultrathin single crystals. Several

groups reported generation of the regular domain patterns with nanoscale periodicity in PZT thin films and $LiTaO_3$ ultrathin crystals using PFM [148, 149]. However, using high-voltage AFM, Molotskii *et al* [114] observed polarization reversal in bulk ferroelectric crystals of lithium niobate. According to them, application of a voltage pulse in the kilovolt range created non-equilibrium conditions for the generated domain by decreasing the depolarization field energy to such an extent that made possible the domain growth in the polar direction in zero-field conditions—an effect that was referred to as domain breakdown. The domain continued to grow until it reached the equilibrium state, i.e. when the energy associated with the increase in the domain surface area compensated the energy change due to the decrease in the depolarization field. Their calculations indicated that for the voltage range that was used, the equilibrium domain length in lithium niobate exceeded the sample thickness ($>150\,\mu$m). Nanodomain patterns were also successfully fabricated in $BaTiO_3$, $Sr_{0.61}Ba_{0.39}Nb_2O_6$ and $RbTiOAsO_4$ single crystals [150, 151].

6.1. High-density data storage

Application of a positive or negative dc bias to the tip can induce 180° polarization switching, orienting polarization upwards or downwards. Thus created domains can be imaged using SPM, which, therefore, provides both 'write' and 'read-out' capabilities. While 'write' operation is performed while contacting the sample surface with a biased tip, the read-out method can be based on PFM or SNDM domain detection, as these approaches provide the highest spatial resolution. Alternatively, domains can be read-out using resistive probes [152, 153]. In this case, the electrostatic field of the written domain depletes or accumulates the carrier inside the low-doped region of the resistive probe. The written domain is detected as a change in the resistance between the two highly doped terminals formed on both sides of the tip. Given that the width of domain walls in ferroelectrics is typically very small (of the order of 1–3 unit cells), this ferroelectric recording potentially allows extremely high data storage density, well above that achievable by conventional magnetic recording. In fact, 40 nm bit size was demonstrated as early as 2002 by Tybell *et al* [11], while a similar level was achieved using magnetic recording by the Wickramasinghe group only in 2004 [154]. Hidaka *et al* [148] proposed to use SPM as a basis for high-density data storage with a PZT thin film as recording media and nanoscale domains as data bits. At the end of 2005, a bit size of 8 nm in diameter corresponding to 10 TBit/inch storage density was demonstrated by Cho *et al* using 40 nm thick single crystals of lithium tantalate [155]. He also showed that the bits in the 128×82 data set could be stored in a statistically reliable way with a bit error rate of 1.8×10^{-2}. These developments generated significant interest from major corporations, such as IBM, Samsung and Canon, towards SPM-based ferroelectric data storage [153].

6.2. Polarity controlled molecular assembling

Polar surfaces of ferroelectrics are characterized by the presence of surface charges and electric potential that can be used in a new set of applications, including local molecular self-assembly, local physical adsorption/desorption, local chemical reactions, local charge transfer reactions and the manipulation of individual organic molecules. First experiments utilizing the effect of ferroelectric polarization on chemical reactivity demonstrated the viability of this approach for assembling of complex nanostructures consisting of oxide substrates, metal nanoparticles and organic/biological molecules [10, 84]. Controllable and selective deposition of molecular and metal species onto nanoscale domain-patterned ferroelectric templates may provide an alternative bottom-up route to lithographic fabrication methods.

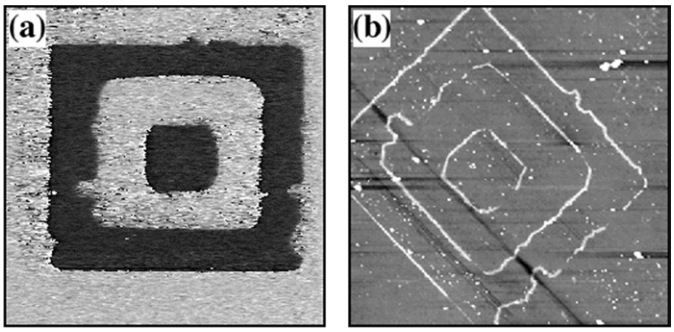

Figure 9. (*a*) PFM image of the tip-generated domain pattern in lithium niobate crystal; (*b*) topographic image showing decoration of domain walls by silver as a result of a photoreduction from aqueous solution. Image in (*b*) is rotated 45° clockwise with respect to (*a*). The scan size is $15 \times 15\,\mu m^2$ [160].

First reports on domain-specific deposition of materials on ferroelectric surfaces governed either by Coulomb interaction or electrochemical reactions were published decades ago [156–158]. In most cases, deposition occurred on the negative or positive ends of domains depending on the sign of the charge carried by the particles or the type of the chemical reaction (reduction or oxidation). Kalinin [10] applied PFM and e-beam to generate nanoscale domain patterns to perform polarity specific deposition of Ag, Rh, Pd and Au metal nanoparticles on $BaTiO_3$ crystals and $Pb(Zr,Ti)O_3$ films via photoreduction from aqueous solution. The mechanism of domain selective is related to semiconductor properties of ferroelectrics and polarization screening, which results in strong band bending on the ferroelectric surface and internal electric field near the interface [159]. Irradiation with band gap light generates electron-hole pairs that are separated in the internal electric field at the interface. Electrons moving to the surface towards the end of the positive domain reduce metal ions, which results in selective metal deposition on pre-determined sites according to the arrangement of positive domains. Fabrication of complex multicomponent structures can be realized by combining this process with chemical reactions used for self-assembling of organic and biological molecules.

Recently, Hanson *et al* [160] showed that the local reactivity on the ferroelectric surfaces depended not only on polarization but also on the balance between polarization charges, adsorbed charges and surface states. Photochemical reduction of silver ions on the surface of domain-patterned $LiNbO_3$ template resulted in silver decoration of 180° domain walls rather than of positive domains (figure 9). This effect was explained by a combination of inhomogeneous distribution of the electric field in the vicinity of the domain wall and low conductivity of the template material. Surface potential, determined by the relative contribution of the external (surface charges) and internal (non-equilibrium carriers) screening mechanisms, is a crucial parameter for assembling molecular structures. Therefore, investigation of the interface properties and deconvolution of the external and internal screening in ferroelectrics is critical for developing new nanofabrication methods using domain-patterned ferroelectric templates.

6.3. Issues related to nanoscale domain engineering

For successful application of this domain-based approach to the development of novel electronic devices and nanofabrication methods several key issues related to the nanoscale domain engineering need to be addressed.

First, reproducibility of high-resolution domain writing is necessary for the fabrication of reliable, large-scale ferroelectric templates. This requirement critically depends on the uniformity of the properties of the ferroelectrics at the nanoscale. This problem can be addressed based on statistical analysis of the PFM data of written domains in thin films [153, 161]. Using this approach the effect of grain size and orientation on spatial homogeneity and reproducibility of the domain writing in thin films has been determined. The same approach can be used for bulk crystals and thin films to investigate the statistical variations in domain sizes as a function of the microstructure of the samples, grain orientation, their dielectric properties and domain writing conditions [122].

Second is the PFM domain writing resolution, i.e. the ability to scale the size of the written domains below 50 nm. There are a number of factors affecting a process of polarization reversal in PFM: microstructure, interface electrical and mechanical conditions, spatial distribution of a tip-generated electric field, etc. Among the factors which are often overlooked but which nevertheless play an important role in the tip-induced ferroelectric switching, are the mechanics of the tip–sample contact and elastic stress exerted by the tip. In the strong tip indentation regime, the combination of mechanical stress and electrical bias allows generation of much smaller domains compared with conventional ferroelectric switching (figure 4) which opens the way for a significant improvement in the writing resolution (<3 nm) [116].

Third, long-term stability of the written domain patterns is a key requirement necessary for fabrication of large-scale nanodomain patterns. This problem is closely related to the problem of thermodynamic stability of the ferroelectric phase at the nanoscale. One of the most important factors affecting domain stability is the screening of spontaneous polarization. EFM and SSPM studies in controlled environment can provide an insight into the process of polarization screening at the nanoscale and will open a way for local stabilization (and destabilization when necessary) of the domain patterns. This combined approach allows quantitative examination of screening processes as a function of time, type of interfaces, template microstructure and surface electronic properties. SPM studies of domains of these dimensions can contribute to a better understanding of the size effects and stability issues in ferroelectrics [155, 162–164].

Fourth, and probably the most serious problem for the use of SPM in nanodomain fabrication, is its low throughput and slow read-out [165], which is limited by the tip scanning rate: while the writing speed in ferroelectrics can be in the nanosecond range, the typical scanning speed of most scanning probe microscopes is in the range of tens of micrometres-per-second. The likely solution of the low throughput lies in the use of massive parallelism as has been recently demonstrated by the IBM Millipede concept [166]. High data rates have been achieved through the use of large (32×32) two-dimensional arrays of SPM probes, which operate simultaneously [153]. Recently, a multiple-tip array has been used to generate a regular one-dimensional domain grating in 200 μm-thick $RbTiOPO_4$ ferroelectric crystals [167]. Another speed limiting factor is the response time of the probe, which measures the interaction force with the sample. Utilizing a special cantilever with a passive mechanical feedback loop operating in the MHz range and a microresonator as a scan stage allows 1000-fold increase in pixel acquisition rate relative to a conventional AFM [168] which is an encouraging development for throughput improvement in the SPM-based fabrication methods.

7. Conclusion

Recent advances in fabrication and characterization of oxide ferroelectrics present both opportunities and challenges. Nanoscale ferroelectric structures have a high potential

for application in electronic devices, such as high-density non-volatile memories. Rapid development of ferroelectric-based devices with reduced dimensions generated a strong need for an extensive investigation of the size effects in ferroelectric materials. Extrinsic effects on polarization stability and mechanism of switching in nanoscale volumes need to be addressed to get an insight into the performance and reliability of nanoscale devices. Scanning probe microscopy techniques provide wide opportunities for studying the physical properties and functionality of ferroelectric materials at the nanoscale level. A possibility of SPM manipulation of ferroelectric domains facilitates development of new nanofabrication approaches and devices. Clearly, the future will evidence broad application of these techniques for ferroelectrics as well as for ferroelectric-semiconductor devices. A quest for the intrinsic limit of the ferroelectric phase requires further theoretical studies that go beyond thermodynamic consideration. It is expected that *ab initio* calculations will play an increasingly important role in understanding the ferroelectric behaviour in one- and two-dimensional nanostructures.

Acknowledgments

One of the authors (AG) acknowledges the financial support of the National Science Foundation (Grant No DMR02-35632, NIRT Grant No 0403871). The authors express their gratitude to R Ramesh, M Alexe, M Shimizu, P Muralt, H Park and F Morrison for kindly allowing the use of their data in this review. J Hanson is acknowledged for providing images of silver nanowires. Numerous interactions and discussions with S V Kalinin are greatly appreciated.

References

[1] Scott J F 2000 *Ferroelectric Memories* (Berlin: Springer)
[2] Waser R (ed) 2005 *Nanoelectronics and Information Technology: Advanced Electronic Materials and Novel Devices* (Berlin: Wiley-VCH)
[3] Uchino K 2000 *Ferroelectric Devices* (New York: Decker)
[4] Dawber M, Rabe K M and Scott J F 2005 *Rev. Mod. Phys.* **77** 1083
[5] Zhirnov V A 1958 *Zh. Eksp. Teor. Fiz.* **35** 1175
Zhirnov V A 1959 *Sov. Phys.—JETP* **35** 832
[6] Onsager L 1944 *Phys. Rev.* **65** 117
[7] Ducharme S, Fridkin V M, Bune A V, Palto S P, BLinov L M, Petukhova N N and Yudin S G 2000 *Phys. Rev. Lett.* **84** 175
[8] Hong S 2003 *Nanoscale Phenomena in Ferroelectric Thin Films* (Dordrecht: Kluwer)
[9] Alexe M and Gruverman A 2004 *Nanoscale Characterization of Ferroelectric: Scanning Probe Microscopy Approach* (Berlin: Springer)
[10] Kalinin S V, Bonnell D A, Alvarez T, Lei X, Hu Z, Ferris J H, Zhang Q and Dunn S 2002 *Nano Lett.* **2** 589
[11] Tybell T, Paruch P, Giamarchi T and Triscone J-M 2002 *Phys. Rev. Lett.* **89** 097601
[12] Terabe K, Nakamura M, Takekawa S, Kitamura K, Higuchi S, Gotoh Y and Cho Y 2003 *Appl. Phys. Lett.* **82** 433
[13] Fong D D, Stephenson G B, Streiffer S K, Eastman J A, Auciello O, Fuoss P H and Thompson C 2004 *Science* **304** 1650
[14] Ganpule C S, Stanishevsky A, Aggarwal S, Melngailis J, Williams E, Ramesh R, Joshi V and de Araujo C P 1999 *Appl. Phys. Lett.* **75** 3874
[15] Luo Y, Szafraniak I, Zakharov N D, Nagarajan V, Steinhart M, Wehrspohn R B, Wendorff J H, Ramesh R and Alexe M 2003 *Appl. Phys. Lett.* **83** 440
[16] Yun W S, Urban J J, Gu Q and Park H 2002 *Nano Lett.* **2** 447
[17] Stanishevsky A, Aggarwal S, Prakash A S, Melngailis J and Ramesh R 1998 *J. Vac. Sci. Technol.* B **16** 3899
[18] Ganpule C S, Stanishevsky A, Su Q, Aggarwal S, Melngaillis J, Williams E and Ramesh R 1999 *Appl. Phys. Lett.* **75** 409

[19] Nagarajan V, Stanishevsky A and Ramesh R 2006 *Nanotechnology* **17** 338
[20] Nagarajan V, Roytburd A, Stanishevsky A, Prasertchoung S, Zhao T, Chen L, Melngailis J, Auciello O and Ramesh R *Nature Mater.* **2** 43
[21] Bühlmann S, Dwir B, Baborowski J and Muralt P 2002 *Appl. Phys. Lett.* **80** 3195
[22] Alexe M, Harnagea C, Hesse D and Gosele U 1999 *Appl. Phys. Lett.* **75** 1793
[23] Harnagea C, Alexe M, Schilling J, Choi J, Wehrspohn R B, Hesse D and Gosele U 2003 *Appl. Phys. Lett.* **83** 1827
[24] Shin H-J, Choi J H, Yang H J, Park Y D, Kuk Y and Kang C-J 2005 *Appl. Phys. Lett.* **87** 113114
[25] Lee S K, Lee W, Alexe M, Nielsch K, Hesse D and Goesele U 2005 *Appl. Phys. Lett.* **86** 152906
[26] Cojocaru C-V, Harnagea C, Rosei F, Pignolet A, van den Boogaart M A F and Brugger J 2005 *Appl. Phys. Lett.* **86** 183107
[27] Alexe M, Scott J F, Curran C, Zakharov N D, Hesse D and Pignolet A 1998 *Appl. Phys. Lett.* **73** 1592
[28] Alexe M, Gruverman A, Harnagea C, Zakharov N D, Pignolet A, Hesse D and Scott J F 1999 *Appl. Phys. Lett.* **75** 1158
[29] Seifert A, Vojta A, Speck J S and Lange F F 1996 *J. Mater. Res.* **11** 1470
[30] Nonomura H, Nagata M, Fujisawa H, Shimizu M, Niu H and Honda K 2005 *Appl. Phys. Lett.* **86** 163106
[31] Fujisawa H, Morimoto K, Shimizu M and Niu H 2000 *Japan. J. Appl. Phys.* **39** 5446
[32] Szafraniak I, Harnagea C, Scholz R, Bhattacharya S, Hesse D and Alexe M 2003 *Appl. Phys. Lett.* **83** 2211
[33] Dawber M, Szafraniak I, Alexe M and Scott J F 2003 *J. Phys.: Condens. Matter* **15** L667
[34] Williams R S, Medeiros-Ribeiro G, Kamins T I and Ohlberg D A 2000 *Annu. Rev. Phys. Chem.* **51** 527
[35] Bühlmann S, Muralt P and Von Allmen 2004 *Appl. Phys. Lett.* **84** 2614
[36] Urban J J, Yun W S, Gu Q and Park H 2002 *J. Am. Ceram. Soc.* **124** 1186
[37] Zhang X Y, Zhao X, Lai C W, Wang J, Tang X G and Dai J Y 2004 *Appl. Phys. Lett.* **85** 4190
[38] Morrison F D, Ramsay L and Scott J F 2003 *J. Phys.: Condens. Matter* **15** L527
[39] Hernandez B A, Chang K-S, Fisher E R and Dorhout P K 2005 *Chem. Mater.* **17** 5909
[40] Hernandez B A, Chang K-S, Fisher E R and Dorhout P K 2002 *Chem. Mater.* **14** 480
[41] Mishina E D, Vorotilov K A, Vasil'ev V A, Sigov A S, Ohta N and Nakabayashi S 2002 *Sov. J. Exp. Theor. Phys.* **95** 502
[42] Agdogan E K, Leonard M R and Safari A 1999 *Handbook of Low and High Dielectric Constant Materials and their Applications* vol 2, ed H S Nalwa (San Diego: Academic) p 61
[43] Kanzig W 1955 *Phys. Rev.* **98** 549
[44] Bachmann R and Barner K 1988 *Solid State Commun.* **68** 865
[45] Shaw T M, Trolier-McKinstry S and McIntyre P C 2000 *Annu. Rev. Mater. Sci.* **30** 263
[46] Streiffer S K, Eastman J A, Fong D D, Thomson C, Mukholm A, Murthy M V R, Auciello O, Bai G R and Stephenson G B 2002 *Phys. Rev. Lett.* **89** 067601
[47] Ginzburg V L and Landau L D 1950 *Zh. Eksp. Teor. Fiz.* **20** 1064
[48] Wurfel P and Batra I P 1976 *Ferroelectrics* **12** 55
[49] Batra I P, Wurfel P and Silverman B D 1973 *Phys. Rev.* B **8** 3257
Batra I P, Wurfel P and Silverman B D 1973 *Phys. Rev.* B **8** 5126
[50] Shih W Y, Shih W H and Aksay I A 1994 *Phys. Rev.* B **50** 15575
[51] Kretchmer R and Binder K 1979 *Phys. Rev.* B **20** 1065
[52] Scott J F, Duiker H M, Beale D, Poulighy P, Dimemr K, Parris M, Butler D and Eaton S 1988 *Physica* B **150** 160
[53] Tsukenawa S, Ishikawa K, Kawazoe Y and Kasuya A 2000 *Phys. Rev. Lett.* **85** 3440
[54] Uchino K, Sadanaga E and Hirose T 1989 *J. Am. Ceram. Soc.* **72** 1555
[55] Catalan G, Noheda B, McAneney J, Sinnamon L J and Gregg J M 2005 *Phys. Rev.* B **72** 0201102
[56] Bratkovsky A M and Levanyuk A P 2005 *Phys. Rev. Lett.* **94** 107601
[57] Bratkovsky A M and Levanyuk A P 2000 *Phys. Rev. Lett.* **84** 3177
[58] Junguera J and Ghosez P 2003 *Nature* **422** 5006
[59] Fu H and Bellaiche L 2003 *Phys. Rev. Lett.* **91** 257601
[60] Kim Y S *et al* 2005 *Appl. Phys. Lett.* **86** 102907
[61] Zembiglotov A G, Pertsev N A, Kohlstedt H and Waser R 2002 *J. Appl. Phys.* **91** 2247
[62] Tybell T, Ahn C H and Triscone J-M 1999 *Appl. Phys. Lett.* **75** 856
[63] Bune A *et al* 1998 *Nature* **391** 874
[64] Terabe K, Nakamura M, Takekawa S, Kitamura K, Higuchi S, Gotoh Y and Cho Y 2003 *Appl. Phys. Lett.* **82** 433
[65] Kalinin S V, Bonnell D A, Alvarez T, Lei X, Hu Z, Shao R and Ferris J H 2004 *Adv. Mater.* **16** 795

[66] See, for example, references in Gruverman A 2004 *Encyclopedia of Nanoscience and Nanotechnology* vol 3, ed H S Nalwa (Los Angeles: American Scientific Publishers) pp 359–75
[67] Martin Y, Williams C C and Wickramasinghe H K 1987 *J. Appl. Phys.* **61** 4723
[68] Stern J E, Terris B D, Mamin H J and Rugar D 1988 *Appl. Phys. Lett.* **53** 2717
[69] Blinov L M *et al* 2001 *J. Appl. Phys*. **89** 3960
[70] Lehnen P, Dec J and Kleemann W 2000 *J. Phys. D: Appl. Phys*. **33** 1932
[71] Luo E Z *et al* 2000 *Phys. Rev.* B **61** 203
[72] Hong J W, Park S-I and Khim Z G 1999 *Rev. Sci. Instrum.* **70** 1735
[73] Eng L M *et al* 1999 *Appl. Surf. Sci*. **140** 253
[74] Tsunekawa S *et al* 1999 *Appl. Surf. Sci.* **137** 61
[75] Hong J W *et al* 1998 *J. Vac. Sci. Technol*. B **16** 2942
[76] Hong J W *et al* 1998 *Phys. Rev*. B **58** 5078
[77] Bluhm H, Wadas A, Wiesendanger R, Roshko A, Aust J A and Nam D 1997 *Appl. Phys. Lett.* **71** 146
[78] Xie Z, Luo E Z, Xu J B, An J, Sundaravel B, Wilson I H, Wang Z Y, Chen X L and Zhao L H 2003 *Phys. Lett.* A **309** 121
[79] Zavala G, Fendler J H and Trolier-McKinstry S 1997 *J. Appl. Phys*. **81** 7480
[80] Martin Y, Abraham D W and Wickramasinghe H K 1988 *Appl. Phys. Lett*. **52** 1103
[81] Nonnenmacher M, O'Boyle M P and Wickramasinghe H K 1991 *Appl. Phys. Lett.* **58** 2921
[82] Bonnell D A and Shao R 2003 *Curr. Opin. Solid State Mater. Sci.* **7** 161
[83] Son J Y, Bang S H and Cho J H 2003 *Appl. Phys. Lett*. **82** 3505
[84] Giocondi J L and Rohrer G S 2001 *Chem. Mater*. **13** 241
[85] Barrett R C and Quate C F 1991 *J. Appl. Phys.* **70** 2725
[86] Rosenthal P A, Yu E T, Pierson R L and Zampardi P J 2000 *J. Appl. Phys.* **87** 1937
[87] Lu X M, Schlaphof F, Grafstrom S, Loppacher C, Eng L M, Suchaneck G and Gerlach G 2002 *Appl. Phys. Lett.* **81** 3215
[88] Luthi R, Haefke H, Meyer K-P, Meyer E, Howald L and Guntherodt H-J 1993 *J. Appl. Phys.* **74** 7461
[89] Eng L M, Friedrich M, Fousek J and Gunter P 1996 *J. Vac. Sci. Technol.* B **14** 1191
[90] Munoz-Saldana J, Schneider G A and Eng L M 2001 *Surf. Sci.* **480** L402
[91] Takashige M *et al* 2000 *Ferroelectrics* **240** 1359
[92] Wang Y G, Dec J and Kleemann W 1998 *J. Appl. Phys*. **84** 6795
[93] Bluhm H, Wiesendanger R and Meyer K-P 1996 *J. Vac. Sci. Technol.* B **14** 1180
[94] Ganpule C S, Nagarajan V, Hill B K, Roytburd A L, Williams E D, Ramesh R, Alpay S P, Roelofs A, Waser R and Eng L M 2002 *J. Appl. Phys*. **91** 1477
[95] Gruverman A, Hatano J and Tokumoto H 1997 *Japan. J. Appl. Phys*. **36** 2207
[96] Wang Y G, Kleemann W, Woike T and Pankrath R 2000 *Phys. Rev*. B **61** 3333
[97] Cho Y, Kirihara A and Saeki T 1997 *Japan. J. Appl. Phys*. **36** 360
[98] Cho Y and Ohara K 2001 *Appl. Phys. Lett.* **79** 3842
[99] Odagawa H and Cho Y 2002 *Appl. Phys. Lett*. **80** 2159
[100] Rabe U, Kopycinska M, Hirsekorn S, Munoz-Saldana J, Schneider G A and Arnold W 2002 *J. Phys. D: Appl. Phys.* **35** 2621
[101] Liu X X, Heiderhoff R, Abicht H P and Balk L J 2002 *J. Phys. D: Appl. Phys*. **35** 74
[102] Rabe U, Scherer V, Hirsekorn S and Arnold W 1997 *J. Vac. Sci. Technol.* B **15** 1506
[103] Tsuji T, Saito S, Fukuda K, Yamanaka K, Ogiso H, Akedo J and Kawakami Y 2005 *Appl. Phys. Lett.* **87** 071909
[104] Tsuji T, Ogiso H, Akedo J, Saito S, Fukuda K and Yamanaka K 2004 *Japan. J. Appl. Phys.* **43** 2907
[105] Yamanaka K and Nakano S 1998 *Appl. Phys.* A **66** S313
[106] Zeng H R, Yu H F, Zhang L N, Li G R, Ding A L, Luo H S and Yin Q R 2005 *Integr. Ferroelectr.* **73** 141
[107] Durkan C, Welland M, Chu D and Migliorato P 2000 *Appl. Phys. Lett.* **76** 366
[108] Harnagea C 2001 *PhD Thesis* Martin-Lüther-Universität Halle, Germany
[109] Kalinin S V 2002 *PhD Thesis* University of Pennsylvania, USA
[110] Hong S, Woo J, Shin H, Jeon J U, Pak Y E, Colla E, Setter N, Kim E and No K 1998 *J. Appl. Phys.* **89** 1377
[111] Kalinin S V and Bonnell D A 2002 *Phys. Rev.* B **65** 125408
[112] Kalinin S V, Karapetian E and Kachanov M 2004 *Phys. Rev*. B **70** 184101
[113] Abplanalp M 2001 *PhD Thesis* Swiss Federal Institute of Technology, Switzerland
[114] Molotskii M, Agronin A, Urenski P, Shvebelman M, Rosenman G and Rosenwaks Y 2003 *Phys. Rev. Lett*. **90** 107601
[115] Molotskii M 2003 *J. Appl. Phys.* **93** 6234
[116] Kalinin S V, Gruverman A, Rodriguez B J, Shin J, Baddorf A P, Karapetian E and Kachanov M 2005 *J. Appl. Phys.* **97** 074305

[117] Morozovska A N and Eliseev E A 2005 *Phys. Status Solidi* b **242** R79
[118] Molotskii M I and Shvebelman M M 2005 *Phil. Mag*. A **85** 1637
[119] Morozovska A N and Eliseev E A 2006 *Physica* B **373** 54
[120] Abplanalp M, Fousek J and Günter P 2001 *Phys. Rev. Lett.* **86** 5799
[121] Shvartsman V V, Pertsev N A, Herrero J M, Zaldo C and Kholkin A L 2005 *J. Appl. Phys.* **97** 104105
[122] Kalinin S V, Gruverman A and Bonnell D A 2004 *Appl. Phys. Lett*. **85** 795
[123] Kholkin A L, Bdikin I K, Shvartsman V V, Orlova A, Kiselev D and Bogomolov V 2005 *MRS Proc*. E **838** O7.6
[124] Wu A, Vilarinho P M, Suchaneck G and Kholkin A L 2005 *Nanotechnology* **16** 2587
[125] Jesse S, Baddorf A P and Kalinin S V 2006 *Appl. Phys. Lett.* **88** 062908
[126] Gruverman A, Auciello O and Tokumoto H 1998 *Annu. Rev. Mater. Sci.* **28** 101
[127] Li J, Nagaraj B, Liang H, Cao W, Lee C H and Ramesh R 2004 *Appl. Phys. Lett.* **84** 1174
[128] Rodriguez B J, Nemanich R J, Kingon A I, Gruverman A, Kalinin S V, Terabe K, Liu X Y and Kitamura K 2005 *Appl. Phys Lett.* **86** 012906
[129] Kholkin A L, Wuthrich Ch, Taylor D V and Setter N 1996 *Rev. Sci. Instrum*. **67** 1935
[130] Dehoff C, Rodriguez B J, Kingon A I, Nemanich R J and Gruverman A 2005 *Rev. Sci. Instrum.* **76** 023708
[131] Gruverman A, Rodriguez B J, Dehoff C, Waldrep J D, Kingon A I, Nemanich R J and Corss J S 2005 *Appl. Phys Lett.* **97** 082902
[132] Ishibashi Y and Takagi Y 1971 *J. Phys. Soc. Japan* **31** 506
[133] Avrami M 1939 *J. Chem. Phys.* **7** 1003
[134] Kolmogorov A N 1937 *Izv. Akad. Nauk USSR; Ser. Math*. **3** 355
[135] Jo W, Kim D C and Hong J W 2000 *Appl. Phys. Lett.* **76** 390
[136] Gruverman A, Tokumoto H, Prakash A S, Aggarwal S, Yang B, Wuttig M, Ramesh R, Auciello O and Venkatesan T 1997 *Appl. Phys. Lett.* **71** 3492
[137] Ganpule C S, Roytburd A L, Nagarajan V, Hill B K, Ogale S B, Williams E D, Ramesh R and Scott J F 2002 *Phys. Rev.* B **65** 014101
[138] Gruverman A, Auciello O and Tokumoto H 1996 *Appl. Phys. Lett.* **69** 3191
[139] Colla E L, Hong S, Taylor D V, Tagantsev A K, Setter N and No K 1998 *Appl. Phys. Lett.* **72** 2763
[140] Kholkin A L, Colla E L, Tagantsev A K, Taylor D V and Setter N 1996 *Appl. Phys. Lett.* **68** 2577
[141] Gruverman A 1997 *JRCAT annual report*
[142] Colla E L, Stolichnov I, Bradely P E and Setter N 2003 *Appl. Phys. Lett.* **82** 1604
[143] Liu J S, Zhang S R, Dai L S and Yuan Y 1995 *J. Appl. Phys.* **97** 104102
[144] Gruverman A, Rodriguez B J, Kingon A I, Memanich R J, Tagantsev A K, Cross J S and Tsukada M 2003 *Appl. Phys. Lett.* **83** 3071
[145] Emelyanov Yu A, Pertsev N A and Kholkin A L 2002 *Phys. Rev.* B **66** 214108
[146] Kholkin A L, Shvartsman V V, Emelyanov Yu A, Poyato R and Pardo L 2003 *Appl. Phys. Lett.* **82** 2127
[147] Gruverman A, Rodriguez B J, Kingon A I, Memanich R J, Tagantsev A K, Cross J S and Tsukada M 2003 *Appl. Phys. Lett.* **83** 728
[148] Hidaka T, Maruyama T, Sakai I, Saitoh M, Wills L A, Hiskes R, Dicarolis S A and Amano J 1997 *Integr. Ferroelectr.* **17** 319
[149] Cho Y, Fujimoto K, Hiranaga Y, Wagatsuma Y, Onoe A, Terabe K and Kitamura K 2002 *Appl. Phys. Lett.* **81** 4401
[150] Terabe K, Takekawa S, Nakamura M, Kitamura K, Higuchi S, Gotoh Y and Gruverman A 2002 *Appl. Phys. Lett.* **81** 2044
[151] Rosenman G, Urenski P, Agronin A, Rosenwaks Y and Molotski M 2003 *Appl. Phys. Lett.* **82** 103
[152] Park H, Jung J, Min D-K, Kim S, Hong S and Shin H 2004 *Appl. Phys. Lett.* **84** 1734
[153] Hong S and Park N 2006 *Scanning Probe Microscopy: Electrical and Electromechanical Phenomena at the Nanoscale* ed S V Kalinin and A Gruverman (Berlin: Springer)
[154] Hamman H F, Martin Y C and Wickramasinghe H K 2004 *Appl. Phys. Lett.* **84** 810
[155] Cho Y, Hashimoto S, Odagawa N, Tanaka K and Hiranaga Y 2005 *Appl. Phys. Lett.* **87** 232907
[156] Person G L and Feldmann W L 1958 *J. Phys. Chem. Solids* **9** 28
[157] Distler G I, Konstantinova V P, Gerasimov V M and Tolmacheva G A 1968 *Nature* **218** 762
[158] Distler G I 1968 *J. Cryst. Growth* **3** 175
[159] Fridkin V M 1979 *Photoferroelectrics* (Berlin: Springer)
[160] Hanson J N, Rodriguez B J, Nemanich R J and Gruverman A 2006 *Nanotechnology* submitted
[161] Gruverman A 1999 *Appl. Phys. Lett.* **75** 1452
[162] Gruverman A and Tanaka M 2001 *J. Appl. Phys*. **89** 1836
[163] Guo H Y, Xu J B, Wilson I H, Xie Z, Luo E Z, Hong S and Yan H 2002 *Appl. Phys. Lett*. **81** 715

[164] Kim D J *et al* 2005 *Appl. Phys. Lett.* **86** 022903
[165] Quate C F 1997 *Surf. Sci.* **386** 259
[166] Vettiger P *et al* 1999 *Microelectron. Eng.* **46** 11
[167] Rosenwaks Y, Dahan D, Molotskii M and Rosenman G 2005 *Appl. Phys. Lett.* **86** 012909
[168] Humphris A D L, Miles M J and Hobbs J K 2005 *Appl. Phys. Lett.* **86** 034106